

Geological Society, London, Special Publications

40Ar/39Ar dating of synkinematic white mica: insights from fluid-rock reaction in low-grade shear zones (Mont Blanc Massif) and constraints on timing of deformation in the NW external Alps

Y. Rolland, M. Rossi, S. F. Cox, M. Corsini, N. Mancktelow, G. Pennacchioni, M. Fornari and A. M. Boullier

Geological Society, London, Special Publications 2008; v. 299; p. 293-315
doi:10.1144/SP299.18

Email alerting service

[click here](#) to receive free email alerts when new articles cite this article

Permission request

[click here](#) to seek permission to re-use all or part of this article

Subscribe

[click here](#) to subscribe to Geological Society, London, Special Publications or the Lyell Collection

Notes

Downloaded by CNRS-INIST on 19 May 2009

$^{40}\text{Ar}/^{39}\text{Ar}$ dating of synkinematic white mica: insights from fluid–rock reaction in low-grade shear zones (Mont Blanc Massif) and constraints on timing of deformation in the NW external Alps

Y. ROLLAND¹, M. ROSSI^{2,3}, S. F. COX⁴, M. CORSINI¹, N. MANCKTELOW⁵,
G. PENNACCHIONI⁶, M. FORNARI¹ & A. M. BOULLIER³

¹*Géosciences Azur, Université de Nice Sophia-Antipolis, CNRS, IRD,
28 Av. Valrose, BP 2135, 06103 Nice, France (e-mail: yrolland@unice.fr)*

²*PGP, University of Oslo, PO Box 1048, Blindern, 0316 Oslo, Norway*

³*LGCA-LGIT, OSUG, BP53, Université J. Fourier, 38041 Grenoble, France*

⁴*Department of Earth and Marine Sciences, and Research School of Earth Sciences,
Australian National University, Canberra, ACT 0200, Australia*

⁵*Geologisches Institut, ETH Zürich, CH-8092 Zürich, Switzerland*

⁶*Dipartimento di Geoscienze, Via Giotto 1, 35137 Padova, Italy*

Abstract: This paper highlights the use of synkinematic white mica, biotite and phlogopite for the dating of deformation in ductile shear zones within crystalline rocks under low-grade metamorphic conditions. The Mont Blanc shear zones range from 1 mm to 50 m in width and have localized intense fluid flow, resulting in substantial differences in mineralogy and whole-rock geochemistry. On the basis of their synkinematic alteration assemblages and geographic distribution within the Mont Blanc Massif, three main metamorphic zones are distinguished within the network of shear zones. These are: (i) epidote ± white mica-bearing assemblages; (ii) chlorite–phlogopite-bearing assemblages; and (iii) white mica ± biotite ± calcite ± actinolite ± epidote-bearing assemblages. $^{40}\text{Ar}/^{39}\text{Ar}$ age spectra of biotite and phlogopite are complex, and reflect significant variations in chemical composition. In biotite, this is partly due to inheritance from precursor Variscan magmatic biotite. In contrast, new white mica grew at the expense of feldspar during Alpine deformation and its Ar spectra do not show any excess ^{40}Ar . On the SE side of Mont Blanc, ages of shear zone phengites have a narrow range of 15.8–16.0 ± 0.2 Ma, which is in the same age range as $^{40}\text{Ar}/^{39}\text{Ar}$ ages of minerals from kinematically related veins. The top-to-SE sense of shear is consistent with initiation of a Mont Blanc flower-structure within a dextral transpressional system by 16 Ma. On the NW side, mini-plateaux ages of 14.5 ± 0.3 and 23.4 ± 0.4 Ma are preserved in the same sample, suggesting the possibility of two phases of deformation. This is also supported by partly preserved ages of 18–36.6 Ma in biotites and phlogopites. Ages between 36 and 18 Ma might reflect ongoing top-to-NW thrusting, following Penninic Front activation, in a context of nappe stacking and crustal thickening. NW-directed thrusting on the NW side of Mont Blanc continued after 18 Ma, synchronous with SE-directed thrusting on the SE side of the massif. These divergent movements produced the overall pop-up geometry of the Mont Blanc Massif, which may correspond to a positive flower structure developed within a zone of regional dextral transpression extending SW from the Rhone valley into the Mont Blanc area.

Mid-crustal shear zones which breach crustal fluid reservoirs can be zones of intense fluid flow during orogenesis, due to deformation-induced permeability enhancement at high pore fluid pressures (e.g., Beach & Fyfe 1972; Beach 1980; Kerrich 1986; Cox *et al.* 1987; O'Hara 1988; Mc Caig *et al.* 1990; Cox 2005). Major redistribution of crustal fluids via transiently permeable shear zone networks may result in significant mass and heat

transport. This in turn can control the stability of mineral assemblages which impact on the rheology of rocks through fluid-present softening reactions, and via effects of fluid pressures on effective normal stresses and frictional shear strength (e.g., Ferry & Gerdes 1998; Guermani & Pennacchioni 1998; Wibberley & McCaig 2000; Cox 2005).

A method for constraining the time of deformation and mineral growth/recrystallization in

shear zones is required to establish the pressure (P)–temperature (T)–time (t) histories during crustal deformation, and to obtain a more complete understanding of how coupling between fluid–rock reaction processes and deformation processes may influence crustal deformation (Ferry & Gerdes 1998; Streit & Cox 1998). The $^{40}\text{Ar}/^{39}\text{Ar}$ dating method is the most frequently used technique for dating low-grade ($T < 450\text{ }^\circ\text{C}$) synkinematic minerals (Kligfield *et al.* 1986; Wijbrans & McDougall 1986; Kelley 1988; Goodwin & Renne 1991; West & Lux 1993; Kirschner *et al.* 1996; Reddy *et al.* 1996), because U–Pb systems close at higher temperatures and the Rb–Sr is prone to resetting by post-deformation fluid circulation (e.g., Wickman *et al.* 1983). In theory, synkinematic minerals formed below their closure temperature retain their crystallization age (e.g., Dodson 1973) and it is generally accepted that direct dating of deformation by $^{40}\text{Ar}/^{39}\text{Ar}$ can be achieved if dynamic crystallization has occurred at or below the closure temperature of a given mineral (West & Lux 1993). However, the interpretation of $^{40}\text{Ar}/^{39}\text{Ar}$ ages obtained for low temperature (LT) shear zone minerals is still a matter of debate. $^{40}\text{Ar}/^{39}\text{Ar}$ ages of synkinematic minerals might date (1) a cooling age corresponding to a specific closure temperature depending on cooling rate and mineral chemistry (T_c ; e.g., Dodson 1973), or (2) a crystallization age, which can approximate the deformation age if crystallization is syntectonic (e.g., Reddy & Potts 1999), or (3) the age of isotopic resetting due to fluid interaction, which can occur both above or below the usually accepted T_c (Villa *et al.* 1997; Villa 1998). Interpretations (1) and (2) are strictly different because the cooling age corresponds to the age at which the rock was cooled below the cooling temperature of the mineral analysed, for example 350–400 $^\circ\text{C}$ for white mica, whereas the crystallization age is not a function of the temperature.

In reality, $^{40}\text{Ar}/^{39}\text{Ar}$ ages might be even more complex, as minerals formed at high temperature (HT) and deformed below T_c might have their Ar-chronometer partly reset due to Ar loss (Hames & Hodges 1993; Hames & Cheney 1997), as suggested by analytical (Kramar *et al.* 2001) and experimental (Dunlap 1997; Dunlap & Kronenberg 2001) work. These studies have emphasized that Ar loss due to diffusion depends on the mineral size and structure, as well as strain intensity and deformation mechanisms. Micas are strongly anisotropic during deformation; they typically deform by dislocation glide parallel to [001] and kinking (Hames & Bowring 1994), as well as by dissolution–precipitation processes. In addition, grain boundary sliding may operate at HT, especially in shear zones (Gibson 1990).

Reddy & Potts (1999) have found that deformation ages can be obtained in cases where deformation has led to a significant change in grain size as the result of dynamic recrystallization. However, $^{40}\text{Ar}/^{39}\text{Ar}$ dating of deformation in low-grade metamorphic systems has been most successfully achieved in cases where micas have grown during deformation, for example in pressure fringes (Sherlock *et al.* 2003). In this case, it may be possible to obtain ages for a specific shearing event and even derive estimates for slip rates in a given shear zone, following the approach of Müller *et al.* (2000).

In this paper, we present the results of $^{40}\text{Ar}/^{39}\text{Ar}$ dating of phyllosilicates (white mica, biotite and phlogopite) formed during the development of a low-grade shear zone network in the Mont Blanc Massif (western Alps). This field example allows comparisons to be made between several $^{40}\text{Ar}/^{39}\text{Ar}$ chronometers formed in the same moderate- to low- T system. The shear zones considered in this study of the Mont Blanc Massif were developed in a suite of relatively homogeneous granite protoliths which differ only in their grain size (Rolland *et al.* 2003; Rossi *et al.* 2005). Various synkinematic, hydrothermal alteration assemblages have developed within the network of granite-hosted shear zones. The nature of the alteration assemblages and changes in rock chemistry during shear zone evolution depend largely on the fluid–rock ratios and chemistry of fluids that migrated through the shear zones under relatively similar PT conditions. The $^{40}\text{Ar}/^{39}\text{Ar}$ dates are discussed in relation to a model for the tectonic–metamorphic–fluid evolution of the Mont Blanc Massif, which is the subject of a larger study (see Rolland *et al.* 2003, 2007; Rossi *et al.* 2005).

Geological setting

Protolith

The Mont Blanc Massif is one of several Variscan ‘External Crystalline massifs’ within the western Alps (Fig. 1) and is composed of paragneisses, orthogneisses, migmatites and granites (Baggio 1958; Ayrton *et al.* 1987; Bussy 1990; Bonin *et al.* 1993). The gneisses have yielded ages of 453 ± 3 Ma, obtained by U–Pb on zircon (Bussy & von Raumer 1994). The Hercynian granite forms a 35×10 km calc-alkaline batholith dated at 300 ± 20 Ma by the Rb–Sr method (Baggio *et al.* 1967; Bussy *et al.* 1989) and at 300 ± 3 Ma by U–Pb on zircon (Bussy & von Raumer 1994). Several magmatic facies have been recognized, mainly based on grain size. The granite facies is porphyritic in the centre of the batholith and becomes very fine-grained near its NW and SE

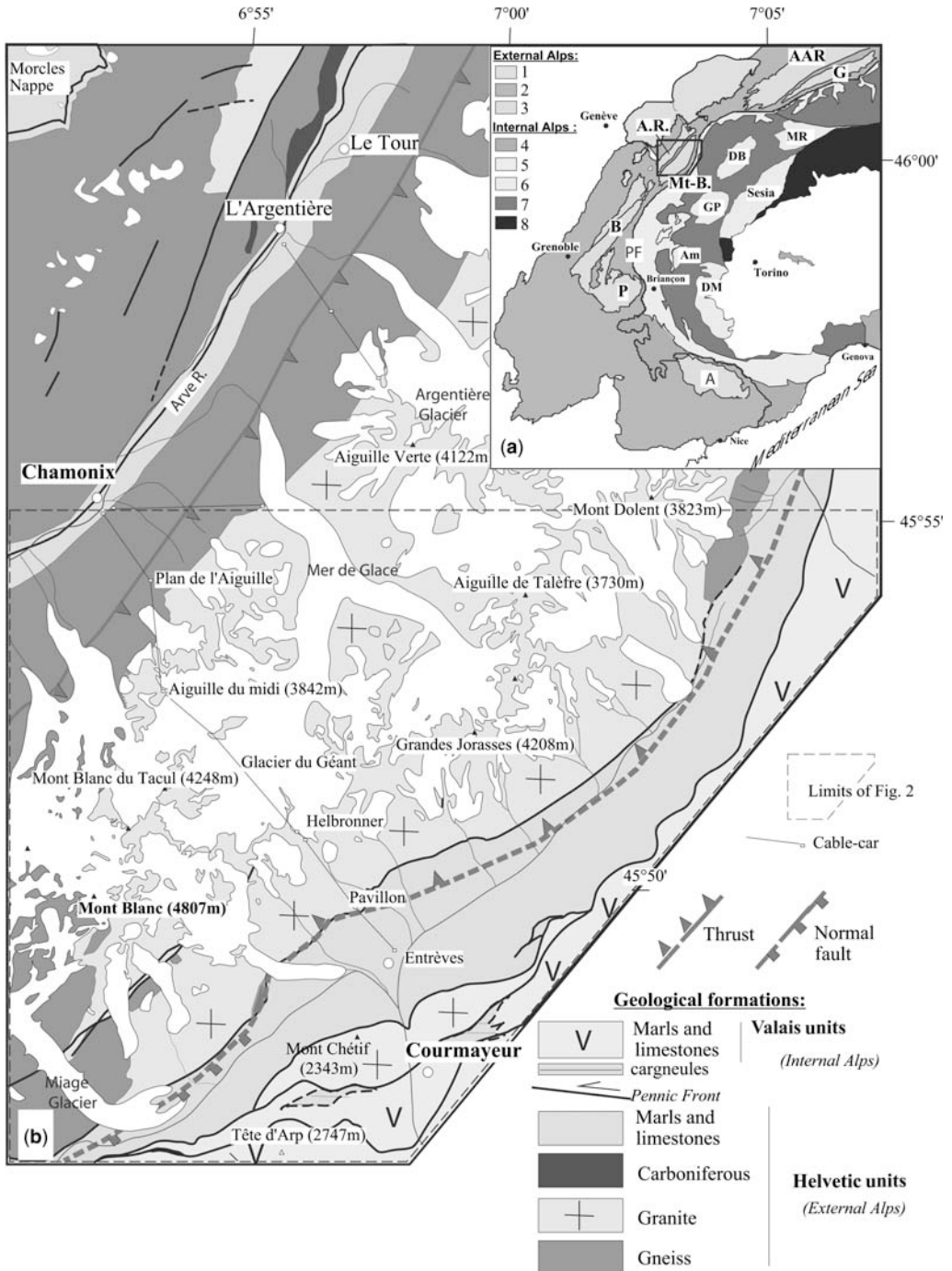


Fig. 1. (a) Geological map of the western Alps. 1, Pre-Alpine nappes; 2, Dauphinois/Helvetic zones; 3, External Crystalline massifs; 4, exotic flysch; 5, Briançonnais zone; 6, Internal Crystalline massifs; 7, Schistes Lustrés complex; 8, Austro-Alpine units of the western Alps. External Crystalline massifs: A, Argentera; AR, Aiguilles Rouges; B, Belledonne; G., Gotthard; Mt-B., Mont Blanc; P., Pelvoux. Internal Crystalline massifs: Am., Ambin; DB., Dent Blanche; GP, Gran Paradiso; MR, Monte Rosa; PF, Penninic Front. **(b)** Simplified geological map of the Mont Blanc Massif, modified after Ayrton *et al.* (1987). The dashed line frames the location of Figure 2.

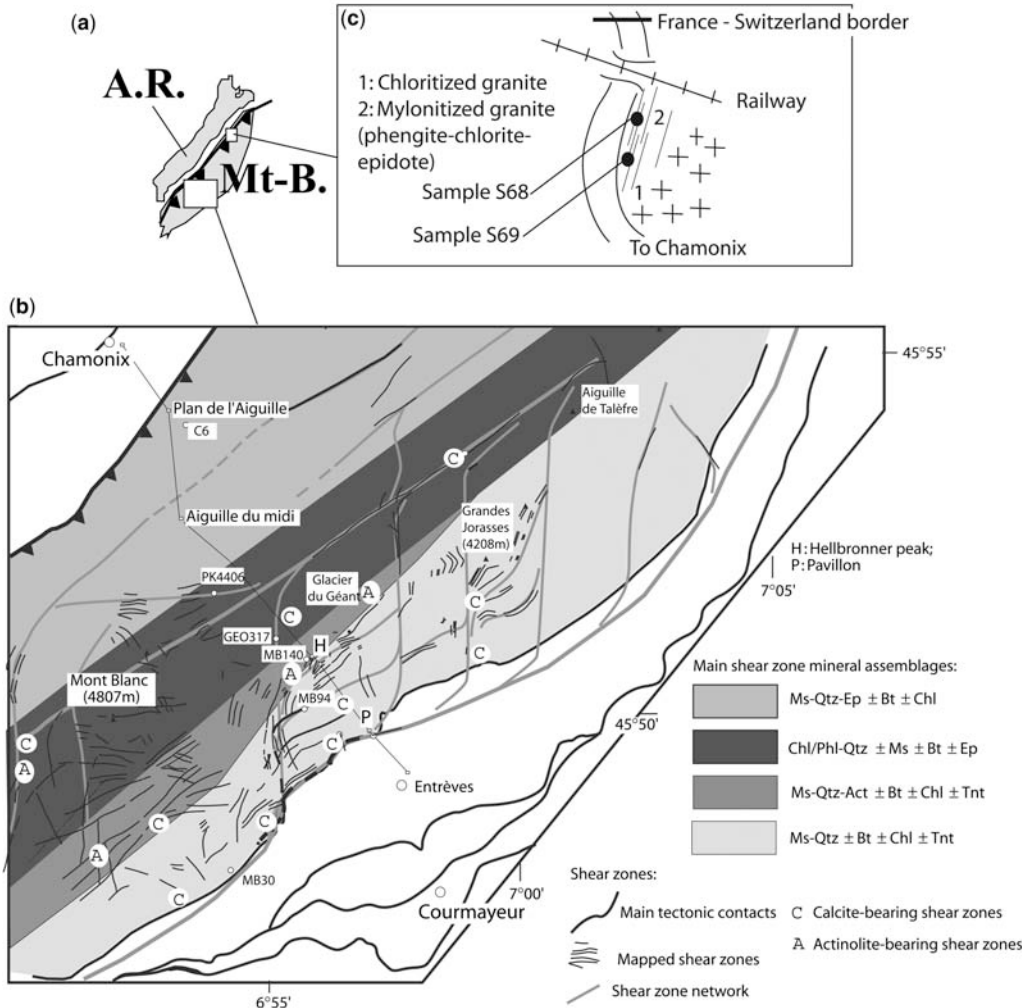


Fig. 2. (a) Location of studied areas in the Aiguilles Rouges–Mont Blanc Massifs. (b) Structural and metamorphic sketch map of the Mont Blanc Massif. Mineral abbreviations: Act, actinolite; Bt, biotite; Chl, chlorite; Ep, epidote; Ms, white mica; Phl, phlogopite; Qtz, quartz; Ttn, titanite; modified after Rossi *et al.* (2005). (c) Sketch of the structural location of samples S68–S69 in the northern part of the Mont Blanc massif, on the border between France and Switzerland.

intrusive contacts with the country rock (Baggio 1958; Marro 1988; Bussy 1990).

Alpine structures

The studied shear zone network in the Mont Blanc Massif has two main components on a regional scale. One trends N40–N60°E with a partly oblique dextral strike–slip sense of shear and the other trends north–south with a partly oblique sinistral strike–slip sense of shear (Fig. 2). The intrusive contacts of the granite were tectonically reactivated during the Cenozoic Alpine orogeny. The massif is

bounded by a NW-vergent thrust on its NW side (e.g., Butler 1985; Belliere 1988) and by a SE-vergent thrust on its SE margin (Antoine *et al.* 1975), and lies within a zone where late (Neogene) regional dextral strike–slip shearing approximately parallel to the SW–NE elongation of the Mont Blanc Massif has also been reported (e.g., Gourlay & Ricou 1983; Hubbard & Mancktelow 1992; Bistacchi *et al.* 2000). The Mont Blanc Massif has been interpreted as: (1) the fold core of the recumbent Morles nappe (e.g., Ramsay 1981; Ramsay *et al.* 1983); (2) an actively extruding pop-up structure as suggested by the

fan-like distribution of faults within the granite (Bertini *et al.* 1985); (3) a back-steepened imbricate slice, with the current SE-directed thrust geometry on the internal side interpreted as an overturned normal fault originally 'accommodating extension on the dorsal culmination wall' (Butler 1985); (4) an uplifted block within a dextral transpressive zone, i.e., a positive flower structure (Gourlay & Ricou 1983; Hubbard & Mancktelow 1992); (5) a recent exhumed within the footwall of a late to recent normal fault on the SE side of the massif (Seward & Mancktelow 1994); and (6) a NW-verging thrust ramp structure with minor back-thrusting to the SE (Leloup *et al.* 2005). On the SE margin of the Mont Blanc, deformation has been shown to evolve with time from a brittle to a ductile style in individual shear zones, due to phyllosilicate recrystallization at the expense of feldspars during fluid-assisted deformation (see Guermani & Pennacchioni 1998). Fluid flow was localized predominantly in shear zones, as well as in kinematically related vein networks (Poty 1969; Marquer 1989; Rolland *et al.* 2003; Rossi *et al.* 2005).

Age of Alpine deformation

The age of shear zone development in the Mont Blanc Massif is poorly constrained. Dating of shear zone minerals has been attempted only for K-feldspar (Leloup *et al.* 2005), which was found to be only partly reset during Alpine (10–20 Ma?) deformation. Ar spectra of K-feldspar were shown to be discordant with step ages ranging between very young (4–20 Ma) and old (300 Ma), interpreted as partial resetting of K-feldspar during the Alpine event. Significant excess ^{40}Ar is interpreted by Leloup *et al.* (2005) to be due to ^{40}Ar inherited from the Variscan magmatic feldspar, which crystallized at *c.* 300 Ma (Bussy & von Raumer 1994). The Alpine white mica–chlorite–epidote–quartz–albite greenschist facies assemblage of the shear zones is interpreted to have been formed between 18 and 36 Ma on the basis of Rb–Sr whole-rock ages (Baggio *et al.* 1967). However, $^{40}\text{Ar}/^{39}\text{Ar}$ dating of biotite from undeformed granites, as well as foliation-defining biotite from weakly deformed granites, provided plateau ages from 22.8 ± 0.6 to 63.7 ± 1.9 Ma. This age range exceeds the range of realistic $^{40}\text{Ar}/^{39}\text{Ar}$ ages for Alpine tectonic events (Leloup *et al.* 2005). The onset of deformation in the External Crystalline Massifs of the Alps should post-date the onset of shearing on the Penninic Front at *c.* 35 Ma (Ceriani *et al.* 2001 and references therein). The Mont Blanc Massif is the basement to the Helvetic sedimentary sequence in the Morcles nappe. The youngest part of this sequence is the Tavayannaz sandstone, which contains andesitic blocks of Periadriatic magmatic age,

i.e., *c.* 32 Ma (Steck 1984; Fischer & Villa 1990). Accordingly, deformation of the Mont Blanc Massif has to be younger than mid-Oligocene, and has usually been assumed to be late Oligocene or early Miocene (Gourlay 1986; Marro 1988). Therefore, excess or inherited ^{40}Ar components are suspected to be present in these >40 Ma samples, and result in apparent ages that are too old. K–Ar dating on minerals from Alpine veins that are kinematically related to shear zones yields ages in the range 15.2–18.3 Ma for adularia (hydrothermal K-feldspar), and in the range 13.4–15.2 Ma for muscovite (Leutwein *et al.* 1970). These ages are close to $^{40}\text{Ar}/^{39}\text{Ar}$ white mica ages of 14.6–18.5 Ma obtained within a thrust affecting the Mont Blanc sedimentary cover in the Morcles Nappe (Crespo-Blanc *et al.* 1995; Kirschner *et al.* 1996, 2003).

P–T estimates of ductile shear zone development

Fluid inclusion studies on granite-hosted vein quartz indicate formation temperatures of 350–400 °C (Poty 1969; Poty *et al.* 1974; Marshall *et al.* 1998). Shear zones were formed under mid-crustal greenschist facies conditions, as shown by estimates of pressure and temperature conditions for shear zone deformation around 0.5 ± 0.05 GPa and 400 ± 25 °C, determined on the basis of independent mineral equilibria (Rolland *et al.* 2003).

Structural and mineralogical setting of studied shear zones

A more detailed analysis of structural, mineralogical and geochemical relationships between the shear zones and the undeformed granite is presented in Rolland *et al.* (2003), Rossi (2005) and Rossi *et al.* (2005). The main features are summarized below.

Shear zone mineralogy

Three main hydrothermal alteration assemblages are recognized, with each main assemblage being developed in distinct geographic domains in the Mont Blanc Massif (Fig. 2b). These assemblages are: (1) white mica \pm actinolite \pm epidote \pm calcite assemblages in the SE part of the massif; (2) chlorite + phlogopite-bearing assemblages in the central part of the massif; and (3) epidote-bearing assemblages in the NW part of the massif (Rolland *et al.* 2003; Rossi *et al.* 2005). The development of the different assemblages from a protolith of near-uniform composition is interpreted to relate to different intensities of fluid–rock interaction within the shear zones, as well as variations in the

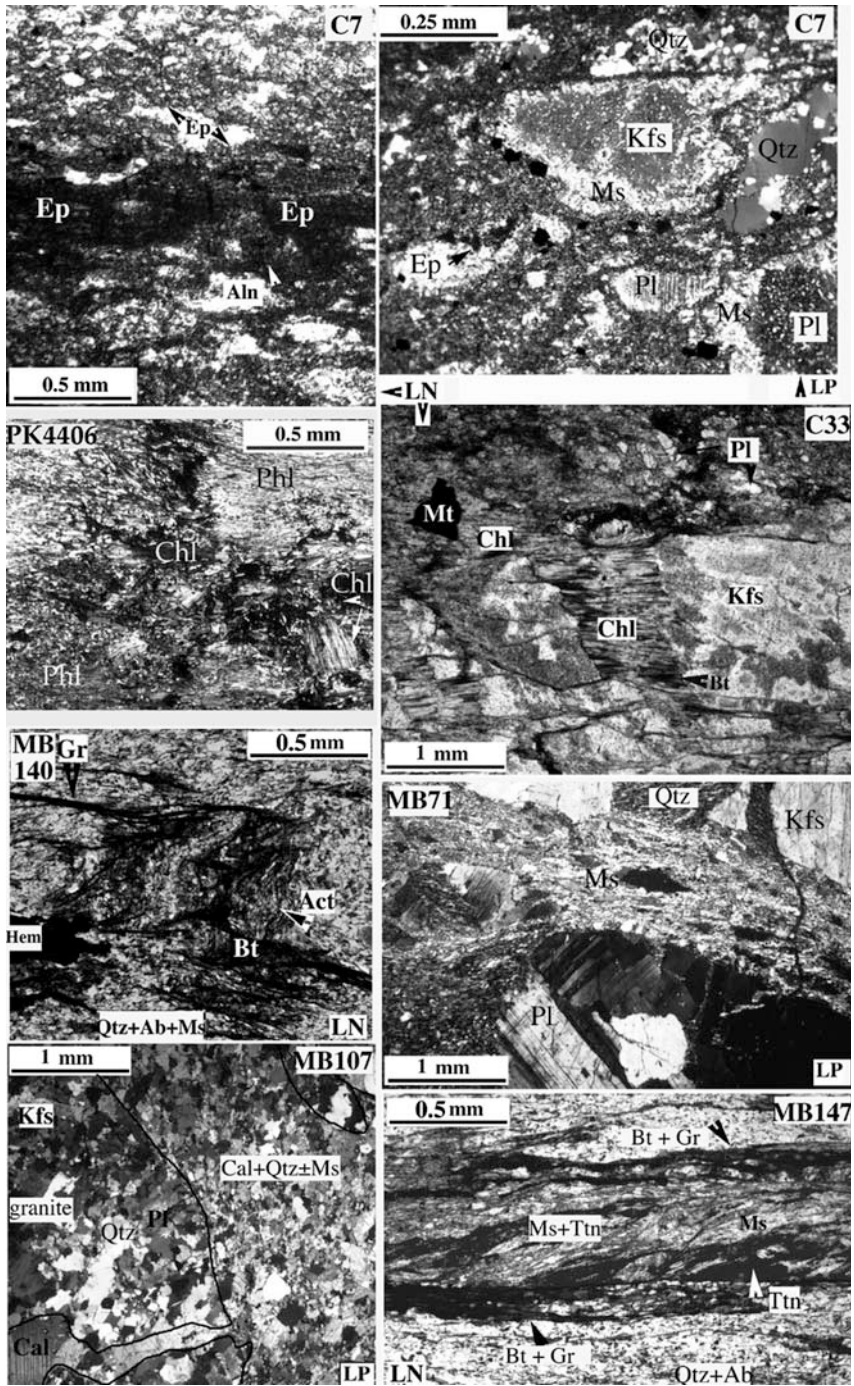
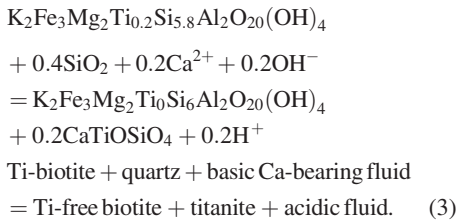
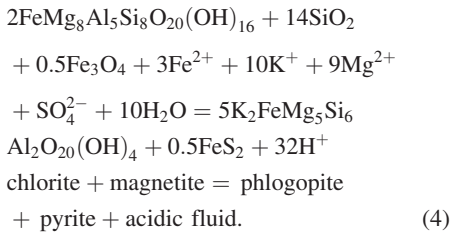


Fig. 4. Photomicrographs of representative mineral assemblages found in the Mont Blanc granite shear zones. Mineral abbreviations, as for Figure 2 and additionally: Ab, albite; Aln, Allanite; Cal, calcite; Gr, graphite; Hem, hematite; Kfs, K-feldspar; Mt, magnetite; Pl, plagioclase. LN, plane polarized light; LP, crossed polars.

domains can be distinguished. These domains are separated by a sharp, but extremely irregular alteration front (Rossi *et al.* 2005). On the basis of S–C fabrics, both top-to-NW and top-to-SE senses of shear are recognized. Accordingly, the bulk deformation pattern is interpreted to be approximately pure shear. The crystallization of chlorite and phlogopite requires substantial Mg-metasomatism during high flux fluid migration within these shear zones. In biotite-rich shear zones, relicts of brown Ti-rich, originally igneous biotite are locally preserved and partially recrystallized into metamorphic green low-Ti biotite by the following reaction:



In most phlogopite-rich samples, phlogopite porphyroblasts have inclusions of relict chlorite, which suggests the following prograde reaction (e.g., sample PK4406, Fig. 4):



Samples for $^{40}\text{Ar}/^{39}\text{Ar}$ dating from phlogopite-rich shear zones in the central and central-east part of the massif were selected from the Mont Blanc tunnel sample collections of the Torino Museum of Natural Sciences (samples PK4406 and GEO317; Fig. 4).

In the NW domain of the Mont Blanc Massif, cataclasites are more common than mylonites. Cataclastic zones are epidote-bearing and there is little neo-crystallization of phyllosilicates and associated transition to ductile shear zones. Epidote forms at the expense of plagioclase, K-feldspar and biotite (e.g., C7, Fig. 4). Biotite crystals were sampled from top-to-NW shear zones (sample C6; Fig. 2) close to the main thrust that forms the NW border of the Mont Blanc Massif. $^{40}\text{Ar}/^{39}\text{Ar}$ dating of shear zone biotite complements biotite $^{40}\text{Ar}/^{39}\text{Ar}$ ages from undeformed granite already published by Leloup *et al.* (2005).

At the French-Swiss border a fine-grained white mica-bearing mylonite (samples S68–69; Figs 2a & 5) was collected within the same top-to-NW thrust zone bounding the Mont Blanc Massif. The fine-grained granite protolith is compositionally similar to the Mont Blanc granite. Deformation within this shear zone has already been described in detail by FitzGerald & Stünitz (1993). In this zone the main top-to-the NW thrust which bounds the Mont Blanc Massif has only one mesoscopically apparent mineral lineation and foliation. However, in thin-section, two foliations are present at a low angle to each other (S1 and S2, Fig. 5). One foliation overprints the other, with each foliation being associated with lattice and shape preferred orientations in phengite aggregates. As these two foliations clearly are not an S–C fabric, they are interpreted

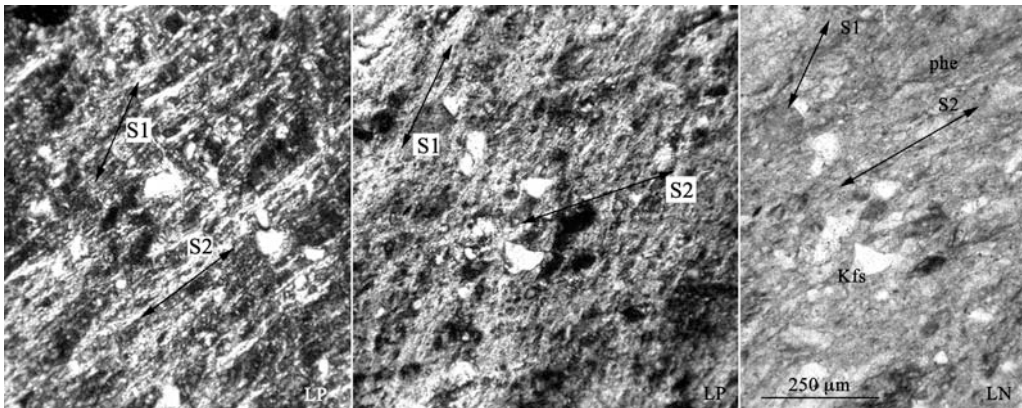


Fig. 5. Photomicrographs of the sample S68 collected At the French–Swiss border (Fig. 2a), within top-to-NW thrust zone bounding the Mont Blanc Massif. S1 and S2 refer to the two generations of phengite evidenced in thin section by rotating the thin section in plane polarized light. Mineral abbreviations: Kfs, K-feldspar; Phe, Phengite. LN, plane polarized light; LP, crossed polars.

as resulting from two separate shearing events. Unfortunately, the two fabrics occur together on such a fine scale that it is not possible to separate grains related to a specific foliation.

Shear zone mineral chemistry

Within individual shear zones, phyllosilicates (chlorite, white mica, biotite–phlogopite) have similar X_{Mg} ($\text{Mg}/\text{Mg} + \text{Fe}$) ratios, indicating good equilibrium between minerals of the synkinematic metamorphic assemblage. On a regional scale, variations in X_{Mg} of the phyllosilicates reflect the observed zoning in metamorphic mineral assemblages present in the shear zones. An inverse bell-shape profile of X_{Mg} values in phyllosilicates is found across the massif, with compositions of $X_{\text{Mg}} = 0.3\text{--}0.1$ at the rim to $X_{\text{Mg}} = 0.9\text{--}0.6$ in the core (Fig. 6). The high X_{Mg} domain coincides with a progressive increase in abundance of mafic minerals toward the central domain of the Mont Blanc Massif. The regional trend is not due to variation in the original composition of the Mont Blanc granite (Rolland *et al.* 2003). Instead, it is interpreted to reflect differences in fluid composition and fluid/rock ratio growth of the phyllosilicates in actively deforming shear zones.

Biotite X_{Mg} compositions in shear zones greatly exceed the range of values exhibited by primary igneous biotites in relatively undeformed granite (Fig. 6). Biotite X_{Mg} ratios in shear zones range between 0.9 and 0.1, whereas in the

undeformed granite X_{Mg} values are approximately 0.4 ± 0.05 (2σ). Phlogopite with $X_{\text{Mg}} = 0.9$ occurs only in shear zones in the central domain of the massif. White mica compositions have homogeneous Si contents of 3.37 ± 0.08 (2σ) per formula unit, based on 84 measurements from samples throughout the massif. Chlorite has X_{Mg} values of 0.3 ± 0.1 near the rim of the massif, whereas high X_{Mg} (0.6 ± 0.1) chlorites are present in the central domain of the massif (Fig. 6 & Table 1).

The three types of alteration assemblages developed in the shear zone network are interpreted in part as a response to varying fluid fluxes across the massif, but they must also reflect the effects of varying fluid chemistry within different parts of the shear network. Chlorite and phlogopite assemblages are developed only in the central domain as a result of high fluid–rock ratios and Mg metasomatism. White mica developed at the expense of feldspars in the SE domain at moderate fluid–rock ratios. Epidote–biotite \pm phengite bearing assemblages in the NW domain suggest limited fluid–rock interaction. This regional variation of alteration assemblages in shear zones provides an opportunity to compare the $^{40}\text{Ar}/^{39}\text{Ar}$ systematics in various micas (phengite, phlogopite and biotite) formed at similar depths but differing fluid–rock interaction environments. It also provides an opportunity to constrain the ages of formation of the various components of the shear network in the Mont Blanc Massif.

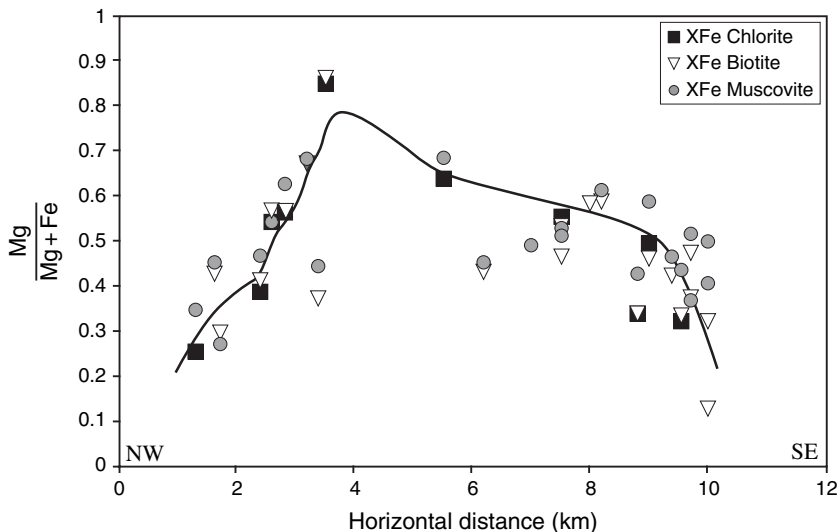


Fig. 6. Mineralogical variation of X_{Mg} ($\text{Mg}/\text{Mg} + \text{Fe}$) values across the Mont Blanc Massif shear zones. Values represent X_{Mg} in each mineral type v. distance. Modified after Rossi *et al.* (2005).

Table 1. Representative analyses of some minerals from the Helbronner area

Major oxides (wt%)	Mineral samples							
	Biotites		Chlorites		White micas			
	MB140	MB02.55D	MB140	MB02.55D	MB140			
SiO ₂	37.33	34.88	26.26	24.53	48.14			
TiO ₂	0.87	1.01	0.09	0.04	0.09			
Al ₂ O ₃	15.29	16.63	19.81	19.19	26.98			
FeO	17.35	23.75	23.09	32.84	3.98			
MnO	0.49	0.50	1.21	1.13	—			
MgO	11.84	8.06	16.82	10.89	2.83			
CaO	0.55	0.00	—	0.07	0.29			
Na ₂ O	—	0.06	—	0.02	—			
K ₂ O	8.24	9.42	0.15	0.01	10.73			
Total	91.96	94.30	87.43	88.72	93.04			
X-Fe	0.45	0.62	0.41	0.63	0.44			
	%vac	3.67	2.50	%Al	25.95	34.14	%Si	3.22
	%Si	86.69	73.41	%Si	67.39	62.23	%Al	61.77
	%Al	9.64	24.08	%diO	6.67	3.63	%Cel	35.01

Biotites: %vac, proportion of di-octaedic biotites; %Si, proportion of the silica-rich biotites (phlogopite – annite); %Al, proportion of aluminium-rich biotites (siderophyllites and eastonite). Chlorites: %Al, proportion of aluminium-rich chlorites; %Si, proportion of silica-rich chlorites; %diO, proportion di-octaedic chlorites. White micas: %Si, proportion of silica-rich muscovite; %Al, proportion of aluminium-rich muscovite; %Cel, proportion of celadonite. MB140, mylonite; MB147, ultramylonite; MB02.55Aa, episyenite; MB02.55D, fresh granite.

⁴⁰Ar/³⁹Ar dating

This section presents new geochronological data obtained on the various sets of shear zones across the Mont Blanc Massif, described in the previous section 8. Results of the laser ⁴⁰Ar/³⁹Ar dating are given in Figures 7 & 8 and Table 2, and procedures are described in the Appendix.

Phengite dating

⁴⁰Ar/³⁹Ar plateau and mini-plateau ages from shear zones on the SE side of the massif range from 15.8 to 16.0 ± 0.2 Ma (Fig. 7a–c). In all samples, the analysed white mica corresponds to a pure mineral, as shown by the corresponding ³⁷Ar_{Ca}/³⁹Ar_K ratio data, except for the highest temperature steps in which the Ca component may result from small mineral inclusions such as epidote (Table 2). Duplicate analyses on samples MB140 and MB94 were undertaken to check data reproducibility and the ages were identical within error (Fig. 7a & b). All three spectra have a staircase shape for lower temperature steps corresponding to 25–50% of cumulative ³⁹Ar, with lower ⁴⁰Ar/³⁹Ar ages at lower temperature. Inverse isochron plots for MB30 and MB94 are not well constrained because of very low ³⁶Ar/⁴⁰Ar, close to detection limits, and a lack of spread in ³⁹Ar/⁴⁰Ar ratios. However, one inverse isochron diagram was obtained for MB140.

It is relatively well constrained and yields a similar age to the plateau age (Fig. 8a).

Near the NW border of the Mont Blanc Massif, the ⁴⁰Ar/³⁹Ar spectra are more complex. Sample S69 does not show a plateau age, whereas S68 shows two mini-plateau ages at 14.3 ± 0.2 Ma (1σ) and 22.9 ± 0.9 Ma (2σ). In Figure 8d, the inverse isochron age of S68 calculated with the first three steps gives a similar age (within error) to the plateau age of 14.5 ± 0.3 Ma. The inverse isochron age obtained with the HT steps (6–8) is 23.4 ± 0.4 Ma, again similar within error to the plateau age for the same HT steps. Both isochron correlations provide (⁴⁰Ar/³⁶Ar)₀ ratios close to the atmospheric value of 295.5, which validates the use of this value in the model calculation of the apparent age steps. As shown on Figure 8f, Ca/K values are between 0.002 and 0.01 for the LT steps, which is within the range of values obtained by microprobe analysis. In HT steps, Ca/K ratios increase to values above those obtained by microprobe analysis, which suggests that other Ca-rich phase(s) may be present as contaminants.

Biotite and phlogopite dating

⁴⁰Ar/³⁹Ar spectra from biotite and phlogopite (Fig. 7f–h) are more irregular. Dating of biotite from the NW part of the massif (sample C6) gives relatively flat Ar spectra with apparent ages

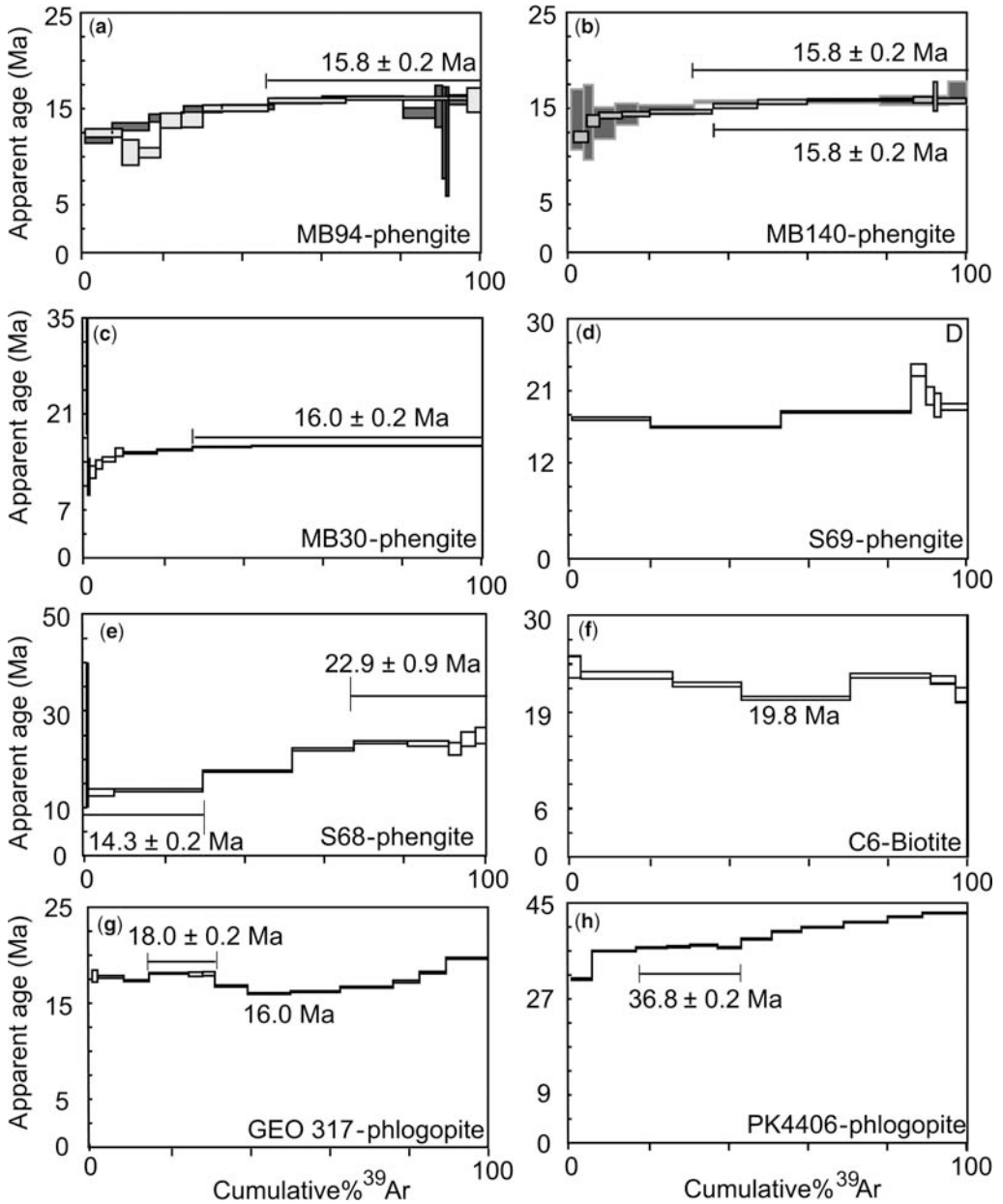


Fig. 7. $^{40}\text{Ar}/^{39}\text{Ar}$ age spectra obtained on mineral separates from shear zone samples of the Mont Blanc Massif (for locations see Fig. 2). Uncertainties on miniplateau and plateau ages are given at the 2σ -level.

between 19.8 and 24 Ma, but no plateau-age can be calculated. The inverse isochron diagram (Fig. 8b) gives an age of 21.8 ± 3 Ma. The 'U' shape of the spectra can be interpreted as an indication of excess ^{40}Ar , as is also suggested by an $(^{40}\text{Ar}/^{36}\text{Ar})_0$ ratio slightly above the atmospheric value. The lower-age step (19.8 Ma) in the central

part of the spectra age could therefore be considered a maximum age for sample C6.

$^{40}\text{Ar}/^{39}\text{Ar}$ spectra of phlogopite from the central-eastern part of the Mont Blanc Massif (sample GEO317, Fig. 7g) are irregular, with step ages between 16 and 20 Ma and a mini-plateau of 18.0 ± 0.2 Ma (1σ) for the LT steps. The inverse

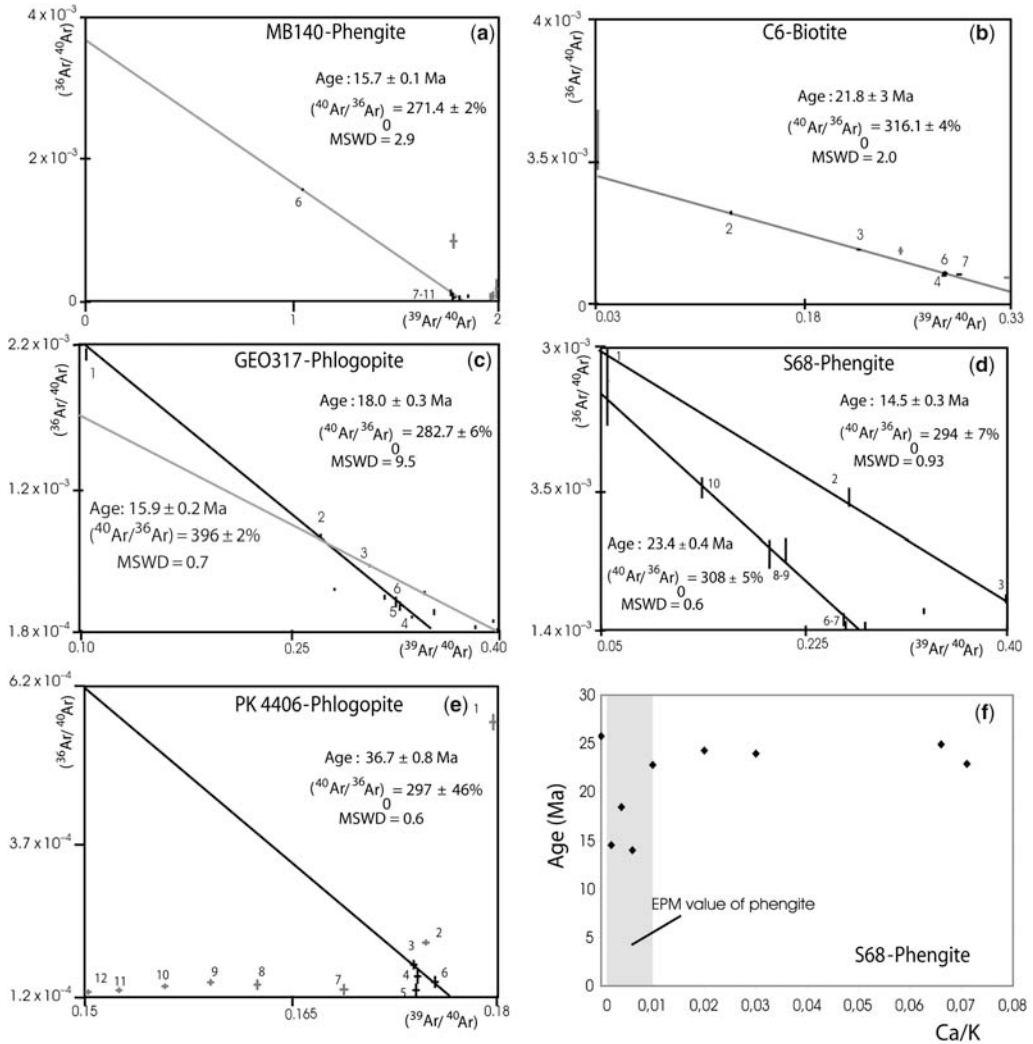


Fig. 8. (a–e) Inverse isochron diagrams of Mont Blanc shear zone samples. (f) Ca/K v. age diagram of phengite from sample S68. MSWD, mean square weighted deviation.

isochron (Fig. 8c) obtained with the same LT steps 1–6 gives the same age, 18.0 ± 0.3 Ma (2σ), with an $(^{40}\text{Ar}/^{36}\text{Ar})_0$ ratio similar to the atmospheric value. An isochron age of 15.9 ± 0.3 Ma (2σ) is calculated for the rest of the spectra. This age is in agreement with the youngest step ages obtained on the $^{40}\text{Ar}/^{39}\text{Ar}$ spectra, as well as with the age of 15.8 Ma obtained in a neighbouring phengite-bearing shear zone (sample MB140). The older ages (>18 Ma) obtained on the HT part of the spectra might be explained by excess ^{40}Ar , as suggested by elevated $(^{40}\text{Ar}/^{36}\text{Ar})_0$ ratios for the 15.9 Ma correlation isochron plot.

Sample PK4406 from the centre of the massif yielded a staircase spectra (Fig. 7h), except for

a mini-plateau obtained in the LT steps at 36.8 ± 0.2 Ma (2σ). A similar age of 36.7 ± 0.8 Ma is obtained from the inverse isochron plot, using the same steps (3, 4, 6), and has an atmospheric $(^{40}\text{Ar}/^{36}\text{Ar})_0$ ratio value. The staircase shape of the spectra at HT is consistent with the presence of excess ^{40}Ar , as shown (Fig. 8e) by increasingly lower ratios between the $^{40}\text{Ar}/^{36}\text{Ar}$ and $^{40}\text{Ar}/^{39}\text{Ar}$ values from step 6 to 12 on the inverse isochron plot.

In summary, for phlogopite-bearing shear zones, older $^{40}\text{Ar}/^{39}\text{Ar}$ ages are found in LT steps (18 Ma for GEO317, 36.6 Ma for PK4406) and excess ^{40}Ar is found in the HT steps.

Table 2. Phengite, biotite and phlogopite $^{40}\text{Ar}/^{39}\text{Ar}$ dating results, from the Mont Blanc shear zones

Step	Laser power (mW)	Furnace temp ($^{\circ}\text{C}$)	Atmospheric cont (%)	^{39}Ar (%)	$^{37}\text{Ar}_{\text{Ca}}/^{39}\text{Ar}_{\text{K}}$	$^{40}\text{Ar}^*/^{39}\text{Ar}_{\text{K}}$	Age (Ma $\pm 1\sigma$)
<i>Sample MB94 (1)</i>							
1	413		20.417	9.37	0.022	0.438	12.464 \pm 0.437
2	441		21.694	4.2	0.033	0.367	10.438 \pm 1.317
3	450		22.243	5.47	0.031	0.366	10.417 \pm 0.514
4	465		2.088	5.29	0.017	0.484	13.76 \pm 0.765
5	481		4.262	5.43	0.016	0.487	13.854 \pm 0.793
6	520		2.481	16.52	0.019	0.53	15.051 \pm 0.326
7	545		1.901	19.6	0.015	0.558	15.849 \pm 0.25
8	576		1.422	30.66	0.026	0.566	16.087 \pm 0.182
9	800		6.42	3.46	0.184	0.56	15.9 \pm 1.268
<i>Sample MB94 (2)</i>							
1	370		18.53	6.86	0.032	0.42	11.90 \pm 0.48
2	388		2.70	9.31	0.031	0.46	13.13 \pm 0.40
3	402		1.02	8.77	0.025	0.50	14.03 \pm 0.41
4	422		0.00	9.64	0.033	0.53	14.95 \pm 0.34
5	432		1.99	13.15	0.036	0.54	15.16 \pm 0.25
6	439		0.47	12.15	0.030	0.56	15.83 \pm 0.28
7	450		0.08	20.50	0.054	0.57	16.15 \pm 0.16
8	455		8.98	8.10	0.069	0.51	14.55 \pm 0.54
9	460		3.14	1.79	0.080	0.54	15.25 \pm 2.18
10	473		16.63	0.90	0.114	0.44	12.50 \pm 4.77
11	501		18.93	0.69	0.200	0.41	11.58 \pm 5.67
12	800		0.85	8.13	0.239	0.56	15.93 \pm 0.50
<i>Sample MB140 (1)</i>							
1	388		32.35	3.24	0.000	0.49	13.85 \pm 3.15
2	410		8.12	2.34	0.010	0.48	13.56 \pm 3.91
3	435		7.10	5.58	0.008	0.47	13.47 \pm 1.66
4	450		1.67	5.78	0.000	0.51	14.41 \pm 1.12
5	475		0.00	14.20	0.006	0.52	14.86 \pm 0.49
6	506		1.28	46.92	0.004	0.55	15.70 \pm 0.14
7	523		2.26	17.25	0.006	0.56	15.82 \pm 0.48
8	700		0.00	4.70	0.015	0.59	16.61 \pm 1.19
<i>Sample MB140 (2)</i>							
1	369		23.75	3.74	0.007	0.43	12.16 \pm 0.56
2	388		4.74	2.84	0.004	0.49	13.78 \pm 0.60
3	408		1.93	6.10	0.006	0.50	14.33 \pm 0.31
4	425		1.76	6.65	0.004	0.51	14.44 \pm 0.23

(Continued)

Table 2. Continued

Step	Laser power (mW)	Furnace temp (°C)	Atmospheric cont (%)	³⁹ Ar (%)	³⁷ Ar _{Ca} / ³⁹ Ar _K	⁴⁰ Ar*/ ³⁹ Ar _K	Age (Ma ± 1σ)
5	439		45.13	16.21	0.003	0.52	14.69 ± 0.19
6	443		1.86	11.50	0.002	0.54	15.27 ± 0.14
7	449		1.33	12.53	0.002	0.55	15.70 ± 0.16
8	455		1.38	26.81	0.004	0.56	15.89 ± 0.09
9	469		1.93	5.42	0.007	0.56	15.89 ± 0.26
10	469		0.00	0.75	0.009	0.57	16.15 ± 1.55
11	1111		3.24	7.44	0.027	0.55	15.75 ± 0.24
<i>Sample S69</i>							
1	379		9.92	19.86	0.000	2.57	17.52 ± 0.19
2	455		2.88	32.94	0.001	2.41	16.47 ± 0.10
3	500		1.71	32.87	0.000	2.69	18.35 ± 0.11
4	525		1.81	3.77	0.007	3.47	23.59 ± 0.76
5	580		—	2.11	0.028	2.99	20.37 ± 1.12
6	680		0.67	1.69	0.003	2.82	19.21 ± 1.48
7	1111		1.09	6.77	0.005	2.79	18.99 ± 0.40
<i>Sample MB30</i>							
1	415		16.51	0.28	0.000	3.89	26.45 ± 8.33
2	435		40.57	0.49	0.002	1.73	11.83 ± 2.66
3	503		25.22	1.54	0.000	1.83	12.52 ± 0.90
4	532		14.98	1.69	0.000	1.99	13.62 ± 0.65
5	555		9.60	3.28	0.000	2.11	14.38 ± 0.35
6	575		2.79	1.94	0.000	2.26	15.43 ± 0.60
7	605		3.61	8.56	0.000	2.25	15.32 ± 0.15
8	627		1.99	8.97	0.000	2.31	15.76 ± 0.11
9	649		1.37	14.89	0.000	2.37	16.19 ± 0.06
10	800		1.80	58.36	0.000	2.39	16.34 ± 0.04
<i>Sample PK 4406</i>							
1	565		17.903	5.15	0.000	4.522	30.733 ± 0.186
2	575		6.368	11.12	0.000	5.305	36 ± 0.1
3	581		5.208	7.85	0.000	5.399	36.63 ± 0.124
4	590		4.604	5.8	0.000	5.425	36.802 ± 0.169
5	605		3.886	6.95	0.000	5.469	37.099 ± 0.156
6	626		4.311	5.99	0.000	5.401	36.644 ± 0.143
7	649		3.914	7.71	0.000	5.641	38.254 ± 0.149
8	672		4.167	7.49	0.000	5.849	39.649 ± 0.138
9	692		4.289	10.69	0.000	5.969	40.454 ± 0.112
10	709		4.082	11.09	0.000	6.112	41.415 ± 0.102
11	726		3.874	8.79	0.000	6.263	42.423 ± 0.109
12	748		3.781	11.37	0.000	6.365	43.108 ± 0.106

Sample GEO317

1	378	61.554	1.34	0.000	2.615	17.834 ± 0.621
2	423	24.658	6.66	0.000	2.602	17.749 ± 0.133
3	444	18.744	6.39	0.000	2.545	17.359 ± 0.089
4	460	8.324	10.01	0.000	2.658	18.125 ± 0.069
5	471	11.413	3.52	0.000	2.643	18.025 ± 0.224
6	491	10.56	3.08	0.000	2.65	18.073 ± 0.203
7	525	13.186	8.28	0.000	2.462	16.794 ± 0.102
8	555	7.504	10.82	0.000	2.346	16.008 ± 0.074
9	581	5.676	12.54	0.000	2.377	16.22 ± 0.074
10	604	6.262	13.39	0.000	2.445	16.68 ± 0.081
11	624	9.321	6.66	0.000	2.531	17.262 ± 0.128
12	678	12.352	6.68	0.000	2.669	18.205 ± 0.118
13	900	13.956	10.62	0.000	2.888	19.689 ± 0.091

Sample C8

1	750	357.657	3.19	0.009	3.493	23.631 ± 1.372
2	850	167.573	22.95	0.001	3.342	22.612 ± 0.442
3	950	179.897	17.27	0.002	3.175	21.49 ± 0.288
4	1050	315.524	27.26	0.001	2.916	19.749 ± 0.212
5	1150	844.847	19.98	0.001	3.33	22.535 ± 0.277
6	1250	2492.416	6.21	0.005	3.257	22.045 ± 0.46
7	1400	1246.793	3.13	0.009	2.977	20.156 ± 0.888

Sample S68

1	650	78.935	0.33	0.000	3.761	25.72 ± 14.638
2	750	44.566	6.67	0.006	2.044	14.026 ± 0.756
3	850	13.509	22.06	0.002	2.115	14.51 ± 0.242
4	950	9.763	22.4	0.004	2.686	18.408 ± 0.2
5	1000	5.307	15.36	0.010	3.337	22.836 ± 0.301
6	1050	5.464	13.5	0.020	3.546	24.259 ± 0.345
7	1100	7.214	10.31	0.030	3.504	23.974 ± 0.537
8	1150	28.362	3.13	0.071	3.348	22.912 ± 1.216
9	1300	27.273	3.6	0.066	3.646	24.937 ± 1.512
10	1450	47.642	2.64	0.275	3.741	25.586 ± 1.615

Discussion

In the literature, $^{40}\text{Ar}/^{39}\text{Ar}$ ages on phyllosilicates are most often interpreted as cooling ages (Dodson 1973), with a closure temperature (T_c) of *c.* 350 °C for white mica and *c.* 300 °C for biotite. However, for low-grade shear zones, this need not necessarily be the case. In this context, minerals are either (i) newly crystallized at the expense of feldspars, or (ii) strained and partly recrystallized during fluid-present shearing. If recrystallization is incomplete, a number of studies have shown that the K–Ar isotopic system is not totally reset (e.g., Kramar *et al.* 2001 and references therein). This is true even if the rocks were buried for a long time at temperatures above the assumed closure temperature for the K–Ar system, and even if the deformation was strongly mylonitic (Kramar *et al.* 2001). As a result, $^{40}\text{Ar}/^{39}\text{Ar}$ ages from phyllosilicates in shear zones could represent (1) the time of syntectonic crystallization, (2) the time of cessation of fluid circulation, (3) the time of cooling through the closure temperature (T_c), (4) a geologically meaningless age reflecting excess or inherited ^{40}Ar , or (5) some indeterminate combination of any of these. In the Mont Blanc Massif, application of the $^{40}\text{Ar}/^{39}\text{Ar}$ chronometer to several different minerals (white mica, biotite and phlogopite) formed during shear zone development by differing amounts of fluid–rock interaction under similar low-T metamorphic conditions provides a chance to critically assess the geological significance of the ages obtained.

Significance of biotite and phlogopite

$^{40}\text{Ar}/^{39}\text{Ar}$ ages

Leloup *et al.* (2005) published five biotite plateau ages from undeformed or slightly deformed Mont Blanc granite, ranging between 22.8 ± 0.6 and 63.7 ± 1.9 Ma. They interpreted these results as cooling ages, except for the older ages, which they considered to have no tectonic significance. In biotite and phlogopite, it is unclear if the old plateau ages are due to (1) significant tectonic events (e.g., cooling through T_c or mineral nucleation at $T \geq 350$ °C), (2) excess ^{40}Ar due to ^{40}Ar incorporation during deformation, or (3) excess ^{40}Ar due to Ar inheritance from magmatic minerals. These three points are now discussed separately.

(1) The fact that biotite shows a range of ages suggests that they do not reflect simple cooling through T_c following Alpine greenschist facies metamorphism. The older Alpine ages reported in the external NW Alps are Upper Eocene–Oligocene (35–30 Ma), and

coincide with the activation of the Penninic Front (Ceriani *et al.* 2001). The external part of the Alps was first involved in Alpine orogenesis at around 35–32 Ma and metamorphic peak conditions could not have been attained before this time. All ages obtained in the current study are close to or younger than this age and therefore could be geologically meaningful. For instance, the LT part of the staircase $^{40}\text{Ar}/^{39}\text{Ar}$ spectra and the corresponding inverse isochron plots yield similar ages, without any evidence for excess ^{40}Ar , of *c.* 18 Ma in sample GEO317 and *c.* 37 Ma in sample PK4406. The 37 Ma age is close to published ages for early NW thrusting along the Penninic Front (Ceriani *et al.* 2001; Dumont *et al.* 2004), while the 18 Ma age is in the range of other phengite ages obtained in the Mont Blanc Massif and the neighbouring external Alps (see below).

(2) It is known that excess ^{40}Ar preferentially partitions into biotite rather than muscovite (Kelley 2002 and references therein). Thus, biotite and phlogopite might be a ‘sink’ for excess ^{40}Ar during fluid–rock interaction. $^{40}\text{Ar}/^{39}\text{Ar}$ biotite age spectra obtained in this study and in Leloup *et al.* (2005) generally show slight U shapes, which could indicate the presence of excess ^{40}Ar (e.g., Arnaud *et al.* 1995; Scaillet 1996). Phlogopite spectra obtained in this study are quite irregular, with old age components (>36.6 Ma for sample PK4406; and ≥ 18.0 Ma for sample GEO317). The inverse isochron plots for both biotite and phlogopite indicate slight (C6, GEO317) to significant excess ^{40}Ar (PK4406). The presence of excess Ar could be related to the growth of phlogopite at the expense of chlorite [reaction (4)], which involves intense Mg-metasomatism with high fluid–rock ratios.

(3) As shown by Rossi *et al.* (2005), the Alpine deformation affects the granite protolith heterogeneously. With increasing deformation in shear zones, pre-existing magmatic minerals are progressively recrystallized under greenschist facies conditions (0.5 GPa and 400 °C; Rolland *et al.* 2003). Under such P – T conditions with incomplete recrystallization of biotite, inherited ^{40}Ar could be partially preserved during Alpine deformation. The $^{40}\text{Ar}/^{39}\text{Ar}$ biotite age must therefore be considered to be a maximum age. The spread of biotite plateau ages from 22.8 ± 0.6 to 63.7 ± 1.9 Ma obtained in undeformed granite by Leloup *et al.* (2005) could well be due to such partial ^{40}Ar inheritance. In the shear zones, (low-Ti)

metamorphic biotite recrystallizes at the expense of (high-Ti) magmatic biotite [reaction (3)]. Unexpelled ^{40}Ar inherited from magmatic biotites is the most likely source of excess Ar, as indicated by older ages obtained in the undeformed granite. Biotites from mylonites, with more intense fluid–rock reaction, yield ages of *c.* 22 Ma, which are within the age range of older phengite ages (sample S68, from the NW part of the massif). If excess ^{40}Ar was introduced by fluids percolating along shear zones, the most deformed rocks should appear older than undeformed rocks (*>c.* 300 Ma, Bussy & von Raumer 1994). As this is not the case, it is probable that the excess ^{40}Ar is inherited from the magmatic biotite.

Significance of white mica $^{40}\text{Ar}/^{39}\text{Ar}$ ages

In contrast to biotite and phlogopite, the Ar spectra obtained for white micas show no evidence of excess ^{40}Ar . Similar ages are obtained on geographically distinct shear zones and on duplicate analyses from the same shear zone.

Explanation for the LT staircase shape of Ar spectra In the SE part of the massif, white mica from samples MB30, 94 and 140 show systematic staircase shapes in the lower-temperature part of Ar spectra. These patterns could be explained by several processes, two of which are considered in detail here.

- (1) The patterns could reflect mixtures and intergrowths between different generations of white mica (Villa *et al.* 1997) or between white mica and other phyllosilicates present as intergrowths, such as paragonite (Boundy *et al.* 1997), illite (DeJong *et al.* 2001) or chlorite (Lo & Onstott 1989). However, different hand-picked white mica separates from the same samples and different samples from separate shear zones have given similar age estimates. Furthermore, electron-microprobe traverses within phengite aggregates have not shown any compositional zoning or the presence of any other K-rich mineral within the aggregates. It is therefore unlikely that the younger ages obtained for the lower temperature steps of the Ar spectra could be due to the presence of mineral inclusions, or to a low-temperature, younger phengite generation in the samples from the SE part of the massif (Fig. 7a–c).
- (2) The patterns could be due to Ar loss, interpreted to result from partial re-opening of

the K–Ar system after crystallization (Berger 1975; Hames & Cheney 1997; McDougal & Harrison 1999). For example, this could be due to post-crystallization deformation of micas (Kramar *et al.* 2001; Mulch *et al.* 2002) or to the effect of late fluids (e.g., Kirschner *et al.* 1996; Villa 1998). Examples of partial Ar resetting due to deformation typically involve large porphyroclasts bordered by microshears (Kramar *et al.* 2001; Mulch *et al.* 2002). This is not the case in SE Mont Blanc massif shear zones, where pressure shadow mica aggregates show no microstructural evidence for subsequent deformation. However, analysis of microtextures in samples MB94 and MB140 from the SE Mont Blanc Massif area and geochemical changes associated with deformation in shear zones from this area indicate that large volumes of fluid have circulated within these shear zones (Rolland *et al.* 2003; Rossi *et al.* 2005). Fluid flow occurred even during the later brittle evolution, as shown by more discrete calcite-bearing, quartz-free veins and quartz-rich cataclasites. Furthermore, present-day high rates of groundwater flow on the order of several cubic metres per second per unit length of fault were measured in the continuation of the MB140 and MB94 shear zones in the underlying Mont Blanc tunnel as it was excavated (Maréchal & Perrochet, 2001). It follows that, in the SE Mont Blanc Massif, the Ar loss observed in the lower temperature steps could be interpreted as being due to post-kinematic fluid circulation (e.g., Kirschner *et al.* 1996).

$^{40}\text{Ar}/^{39}\text{Ar}$ spectra with LT and HT mini-plateaux In the NW part of the massif, sample S68 shows an irregular Ar spectra, with two miniplateaux at LT (14.3 ± 0.2 Ma) and HT (22.9 ± 0.9 Ma). Unlike phengites from the SE part of the massif, the staircase shape is interpreted as reflecting two distinct events, with the ^{40}Ar loss ascribed to a superposed crystallization event and not to post-kinematic fluid circulation. Textural observations from sample S68 show that two foliations are present, in agreement with a two-phase evolution and the development of two phengite generations at (1) *c.* 23 Ma and (2) *c.* 14 Ma, respectively. In similar Alpine settings, such spectra were interpreted by Kirschner *et al.* (1996) and Markley *et al.* (1998) to reflect superposed shearing events within the same zone. This possibility is also supported by the presence of U-shaped Ca/K ratios, interpreted by Wijbrans & McDougall (1986) and DeJong (2003) as being due to the presence of chemically

inhomogeneous mica that was incompletely recrystallized during a younger deformation event.

Cooling or nucleation age? In large crystals (*c.* 500 μm), the closure temperature T_c for the K–Ar white mica system (*c.* 350–450 °C) is slightly above that of phlogopite (*c.* 300–350 °C, e.g., Villa 1998; West & Lux 1993). For a cooling rate of 25 °C Ma^{-1} deduced from the age of 16 Ma obtained by phengite Ar–Ar dating and the temperature of 400 °C obtained by thermobarometry, we recalculate T_c for the size of mica grains in the analysed shear zone aggregates (*c.* 50 μm) with the diffusion parameters of Hames & Bowring (1994). This yields an estimate of $T_c = 338$ °C for white mica and $T_c = 278$ °C for biotite and phlogopite. If we assume that $^{40}\text{Ar}/^{39}\text{Ar}$ ages are cooling ages, white mica should be older than biotite and phlogopite. In the case of the Mont Blanc Massif, white mica ages are much younger than biotite and phlogopite ages. For a cooling rate of 25 °C Ma^{-1} , a difference in T_c of 50 °C would lead to an age difference of 2 Ma, far above the error span of ± 0.2 Ma. In contrast, biotite and phlogopite ages are systematically older than phengite by more than 2 Ma. Thus, the consistent ages obtained between different phengite samples more likely represent the age of synkinematic crystallization during a short-lived shearing event, rather than cooling ages. However, if the ages obtained for phengite were cooling ages, then the phengite could still only have grown at a temperature slightly above T_c , because the maximum temperature reached in the Mont Blanc Massif during Alpine deformation was around 400 °C. In this case, $^{40}\text{Ar}/^{39}\text{Ar}$ dating of phengite provides a minimum age of deformation, but, because of the fast cooling rate of *c.* 25 °C Ma^{-1} the cooling age should be only *c.* 2 Ma younger than the crystallization age.

Age of deformation in the Mont Blanc massif

As discussed above, phengite develops by feldspar breakdown [reactions (1) and (2)] and crystallizes in strain shadows and foliation domains around feldspar porphyroclasts, parallel to the stretching lineation (on average pitching $W70^\circ$ on a $N45^\circ\text{E}–70^\circ\text{N}$ foliation plane, see also Guermani & Pennacchioni 1998). The asymmetric development of these strain shadows (Fig. 3) is consistent with the overall kinematic indicators indicating top-to-SE sense of shear on the SE side and top-to-NW on the NW side of the Mont Blanc Massif, with a smaller dextral component (lineations plunge $60–90^\circ$; Rossi *et al.* 2005). The age of the three analysed shear zones from the SE area

(i.e., MB94, MB140 and MB30) varies by less than 0.2 Ma, i.e., it is effectively the same within error. Top-to-SE motion therefore initiated at or before *c.* 16 Ma on the SE side of the Mont Blanc Massif (if the 18 Ma phengite age is interpreted as a cooling age, with rapid cooling of *c.* 25 °C Ma^{-1} , see above). This result is in agreement with previous K–Ar ages from horizontal vein minerals which are kinematically related to the shear zones, yielding 15.2–18.3 Ma on adularia and 13.4–15.2 Ma on muscovite (Leutwein *et al.* 1970).

Deformation in the central-western part of the Mont Blanc Massif is less well constrained, but two ages of 22.9 ± 0.9 and 14.3 ± 0.2 Ma were obtained on sample S68. As discussed above, these two ages may represent two deformation phases in the same shear zone. As only top-to-NW sense of shear has been observed in this shear zone, it is likely that both deformation events are due to thrusting towards the NW. The LT miniplateau age of 14.3 Ma is relatively close to the age of 15.8 Ma obtained from shear zones on the SE side of Mont Blanc Massif and to the K–Ar ages obtained by Leutwein *et al.* (1970) on kinematically related veins. The age of 22.9 Ma for the higher-temperature mini-plateau from this phengite sample is close to younger biotite ages (22.8 ± 0.6 Ma) obtained in the ‘undeformed granite’ by Leloup *et al.* (2005), and also close to that for biotite sampled from a shear zone close to the thrust on the NW border of the Mont Blanc Massif (21.8 ± 3 Ma). The $^{40}\text{Ar}/^{39}\text{Ar}$ ages of samples S68 and S69 therefore suggest that this NW-directed thrusting was first active at around 22–23 Ma, but was probably later reactivated, with movement continuing down to *c.* 14 Ma. Near-simultaneous deformation on both sides of the massif at 14–16 Ma is in agreement with the interpretation of the Mont Blanc Massif as a pop-up structure, as proposed earlier by Von Raumer (1974) and Bertini *et al.* (1985). However, as noted above, there is also evidence for an overall dextral component to deformation on both sides of the Mont Blanc Massif (Gourlay & Ricou 1983; Hubbard & Mancktelow 1992; Bistacchi *et al.* 2000; Rossi *et al.* 2005), which would suggest that this pop-up is more of a positive flower structure within a dextral transpressive zone, although the dextral component need not be large (Rossi *et al.* 2005). Based on the $P–T–t$ data, the massif has been exhumed at a continuous rate of *c.* 1 mm/year since 16 Ma, which is the rate obtained using both $^{40}\text{Ar}/^{39}\text{Ar}$ data and FT data (Seward & Mancktelow 1994; Leloup *et al.* 2005). Based on these new data and the lack of any jump in FT ages across the Mont Blanc Massif, we propose that the tectonic context of the Mont Blanc Massif has not changed significantly since 16 Ma.

Significance of Mont Blanc deformation ages in the framework of the western Alps

The ages older than 16 Ma can be related to deformation during nappe transport (cf. age data on the Morcles Nappe from Kirschner *et al.* 1996). Nappe transport in the external Alps probably began with activation of the Penninic Front and related thrusts (Ceriani *et al.* 2001), subsequent to deposition of the Taveyannaz sandstone around 32 Ma (Fischer & Villa 1990). In the Mont Blanc Massif, an apparent age of 36.6 Ma is obtained in sample PK4406 phlogopites, but this age is probably not geologically meaningful, due to some excess ^{40}Ar component. Most $^{40}\text{Ar}/^{39}\text{Ar}$ ages, such as the S68 phengite age of 22.9 ± 0.9 Ma, the younger biotite ages from Leloup *et al.* (2005) and our biotite–phlogopite data (sample C6 biotite, GEO 317 phlogopite), indicate an early phase of top-to-NW thrusting starting at 23–24 Ma and continuing to around 16–18 Ma. This phase of thrusting is correlated with the emplacement of the Morcles/Doldenhorn nappe (Crespo-Blanc *et al.* 1995; Kirschner *et al.* 1999, 2003). The younger ages around 16 Ma are interpreted as representing the transition to a phase of backfolding and backthrusting in the Alps, as already proposed by Hunziker *et al.* (1992) and Kirschner *et al.* (2003). This later period is also associated with truncation of nappes in the Rhone Valley by the dextral transcurrent Rhone–Simplon fault (Steck 1984; Mancktelow 1992; Burkhard 1990; Steck & Hunziker 1994). The transpressive pop-up structure of the Mont Blanc developed within the westward continuation of this Rhone–Simplon dextral fault system (Hubbard & Mancktelow 1992), which has been active since *c.* 18 Ma (Grasemann & Mancktelow 1993).

Conclusions

Constraining the age of ductile deformation events in the middle to upper crust (e.g., in the Mont Blanc massif) necessitates dating minerals that crystallized during deformation at or below their closure temperature T_c . The P – T – t data for key deformation events can be obtained by combining thermobarometry with $^{40}\text{Ar}/^{39}\text{Ar}$ dating on newly grown minerals that have crystallized synkinematically and actually provide the kinematic indicators to determine the sense-of-shear (e.g., asymmetric pressure shadows or S–C structures). In this study, direct dating of shear zone deformation was undertaken for a set of synkinematic minerals (white mica, biotite and phlogopite) formed at 0.5 ± 0.05 GPa and 400 ± 25 °C in the Mont Blanc Massif shear zone network, which is

interpreted to represent a dextral transpressive pop-up system.

Biotite and phlogopite crystals preserve significant amounts of inherited and possibly excess ^{40}Ar , but some geologically significant ages have been obtained in the LT part of Ar spectra, ranging between 36.6 and 18.0 Ma. In the NW part of the massif, $^{40}\text{Ar}/^{39}\text{Ar}$ biotite ages are locally similar to phengite ages, ranging between 21.8 and 22.9 Ma. In contrast, in the SE part of the massif, white mica (phengite) provides undisturbed younger ages, with no evidence for excess ^{40}Ar . The absence of any excess ^{40}Ar in phengite is ascribed to the nucleation of phengite at the expense of feldspars during low to moderate fluid/rock ratio deformation. In contrast, biotite nucleates on and replaces pre-existing magmatic biotite. Phlogopite may have incorporated some excess ^{40}Ar during high fluid–rock ratio deformation. In the case of multiple shearing events within a single shear zone, the $^{40}\text{Ar}/^{39}\text{Ar}$ phengite age provides either (1) disrupted age spectra, with step ages ranging between the maximum age of the second tectonic event and the minimum age of the first event (sample S69), or (2) miniplateaux, which could possibly represent the age of each event (sample S68). In the case of single events, well-defined single plateau ages are obtained, such as in the SE part of the Mont Blanc Massif. In this area, ages are all within 15.8–16.0 Ma, in agreement with ages previously determined on vein mineral assemblages whose formation was associated with shear zone development. Partial ^{40}Ar loss could be associated with late fluid circulation, but does not significantly affect the estimated plateau ages. In conclusion, phengite can be a good tool for estimating deformation ages in structurally well-defined low-grade shear zones, if carefully constrained by a combination of field observation, microstructural analysis, geochemistry and geothermobarometry.

This research was supported partly by an Australian Research Council grant. The authors wish to thank G. Féraud for his help with $^{40}\text{Ar}/^{39}\text{Ar}$ laser dating, the Torino Museum of Natural Sciences for providing samples from the Mont Blanc tunnel, and K. DeJong and S. Sherlock for their careful and stimulating reviews.

Appendix: analytical techniques

Locations of the samples dated by $^{40}\text{Ar}/^{39}\text{Ar}$ are provided in Table 3. Mineral compositions were determined by electron probe microanalysis (EPMA). The analyses were carried out at 15 kV and 1 nA using a Jeol 6400 scanning electron microscope (SEM) equipped with an Oxford Instrument light EDS detector and Link ISIS SEMquant software, at the ANU Electron Microscopy Unit. Natural

Table 3. GPS coordinates (UTM-WGS84) and tunnel location of samples dated by $^{40}\text{Ar}/^{39}\text{Ar}$

Sample	GPS (N)	GPS (E)
C6	5084725	335411
MB30	5076035	336641
MB94	5077445	339523
MB140	5079122	339420
S68 & S69	5101734	341103
PK4406	4.406 km in Mont Blanc tunnel (from entrance on the French side)	
GEO317	6.334 km in Mont Blanc tunnel (from entrance on the French side)	

samples were used as standards. Representative mineral analyses are presented Table 1. The textural relationships between the minerals in each assemblage suggest a series of reactions occurring during deformation. Reactions (1)–(4) are written assuming Al mobility, as supported by mass-balance calculations in Rossi *et al.* (2005). The mineral formulae used are approximated following representative EPMA analyses (Table 1).

Geochronology of synkinematic micas was undertaken by laser $^{40}\text{Ar}/^{39}\text{Ar}$ dating. Results are presented in Table 2. White mica was analysed by EPMA to check that mineral compositions are homogeneous from core to rim. Grain aggregates less than 1 mm were separated by hand-picking under a binocular microscope, to avoid altered grains. The samples were then irradiated in the nuclear reactor at McMaster University in Hamilton (Canada), in position 5c, along with Hb3gr hornblende neutron fluence monitor, for which an age of 1072 Ma is adopted (Turner *et al.* 1971). The total neutron flux density during irradiation was 9.0×10^{18} neutron/cm². The estimated error bar on the corresponding $^{40}\text{Ar}^*/^{39}\text{Ar}_k$ ratio is $\pm 0.2\%$ (1σ) in the volume where the samples were set.

Analyses of small amounts of mica aggregates (1 aggregate of c. 500 μm and 2–4 mg: samples MB30, MB94, MB140, GEO317 and PK4406) were undertaken by step heating with a 50 W CO₂ Synrad 48-5 continuous laser beam. Measurement of isotopic ratios was done with a VG3600 mass spectrometer, equipped with a Daly detector system. Detailed procedures are given in Jourdan *et al.* (2004). The typical blank values for extraction and purification of the laser system are in the ranges 4.2–8.75, 1.2–3.9 and 2–6 cc STP for masses 40, 39 and 36, respectively. Analyses of larger mica populations (10 aggregates of c. 500 μm and c. 20–40 mg: samples S68 and C8) were undertaken with a furnace step-heating technique using a double-vacuum high-frequency furnace and a mass spectrometer composed of a 120° MASEE tube, a Baur–Signer GS98 source and a Blazers electron multiplier. Heating lasted 20 min for each temperature step, followed by 5 min for clean-up of the released

gas, before introducing the gas into the spectrometer. Ar isotopes were of the order 100–2000, 100–1000 and 2–200 times the blank for masses 40, 39 and 36, respectively. All measurements were undertaken at the University of Nice (Géosciences Azur). For both Ar-dating techniques, the mass-discrimination was monitored by regularly analysing air pipette volume. Decay constants are those of Steiger & Jäger (1977). Uncertainties on apparent ages are given at the 2σ level and do not include the error on the $^{40}\text{Ar}^*/^{39}\text{Ar}_k$ ratio of the monitor.

The criteria generally used in the laboratory for defining a ‘plateau’ age are the following: (1) it should contain at least 70% of total ^{39}Ar released; (2) there should be at least three successive step-heating fractions in the plateau; (3) the integrated age of the plateau (weighted average of apparent ages of individual fractions comprising the plateau) should agree with each apparent age of the plateau with a 2σ error. In this study, we also consider plateaux smaller than 70% of total ^{39}Ar , because the lower temperature age spectra are generally lowered by a ^{39}Ar loss effect.

References

- ANTOINE, P., PAIRIS, J. L. & PAIRIS, B. 1975. Quelques observations nouvelles sur la structure de la couverture sédimentaire interne du massif du Mont Blanc, entre le Col du Ferret (frontière italo-suisse) et la Tête des Fours (Savoie, France). *Géologie Alpine*, **51**, 5–23.
- ARNAUD, N. O. & KELLEY, S. P. 1995. Evidence for excess argon during high pressure metamorphism in the Dora Maira Massif (Western Alps, Italy), using an ultra-violet laser ablation microprobe ^{40}Ar – ^{39}Ar technique. *Contributions to Mineralogy and Petrology*, **121**, 1–11.
- AYRTON, S., BARFÉTY, J. C., BELLIERE, J., GUBLER, Y. & JEMELIN, L. 1987. *Carte géologique de Chamoni* (1/50 000). BRGM, Orléans.
- BAGGIO, P. 1958. Il granito del Monte Bianco e le sue mineralizzazioni uranifere. *Studi e ricerche della divisione geomineraria CNRN Roma*, **1**, 1–130.
- BAGGIO, P., FERRARA, G. & MALADORA, R. 1967. Results of some Rb/Sr age determinations of the rocks of the Mont Blanc tunnel. *Bollettino della Società Geologica Italiana*, **86**, 193–212.
- BEACH, A. 1980. Retrogressive metamorphic processes in shear zones with special reference to the Lewisian complex. *Journal of Structural Geology*, **2**, 257–263.
- BEACH, A. & FYFE, W. S. 1972. Fluid transport in shear zones at Scourie, Sutherland: evidence of overthrusting? *Contributions to Mineralogy and Petrology*, **36**, 175–180.
- BELLIERE, J. 1988. On the age of mylonites within the Mont Blanc massif. *Geodinamica Acta*, **2**, 13–16.
- BERGER, G. W. 1975. $^{40}\text{Ar}/^{39}\text{Ar}$ step heating of thermally overprinted biotite, hornblende and potassium feldspar from Eldora, Colorado. *Earth and Planetary Science Letters*, **26**, 387–408.
- BERTINI, G., MARCUCCI, M., NEVINI, R., PASSERINI, P. & SGUAZZONI, G. 1985. Patterns of faulting in the Mont Blanc granite. *Tectonophysics*, **111**, 65–106.

- BISTACCHI, A. EVA, E., MASSIRONI, M. & SOLARINO, S. 2000. Miocene to Present kinematics of the NW-Alps: evidences from remote sensing, structural analysis, seismotectonics and thermochronology. *Journal of Geodynamics*, **30**, 205–228.
- BONIN, B., BRÄNDLEIN, P. *ET AL.* 1993. Late Variscan magmatic evolution of the Alpine basement. In: VON RAUMER, J. F. & NEUBAUER, F. (eds) *Pre-Mesozoic Geology in the Alps*. Springer, Heidelberg, 171–201.
- BOUNDY, T. M., HALL, C. M., LI, G., ESSENE, E. J. & HALLIDAY, A. N. 1997. Fine-scale isotopic heterogeneities and fluids in the deep crust: a $^{40}\text{Ar}/^{39}\text{Ar}$ laser ablation and TEM study of muscovites from a granulite–eclogite transition zone. *Earth and Planetary Science Letters*, **148**, 223–242.
- BURKHARD, M. 1990. Aspects of the large-scale Miocene deformation in the most external part of the Swiss Alps (Subalpine Molasse to Jura fold belt). *Eclogae Geologicae Helvetiae*, **83**, 559–583.
- BUSSY, F. 1990. *Pétrogenèse des enclaves microgrenues associées aux granitoïdes calco-alcalins: exemple des massifs varisque du Mont Blanc (Alpes occidentales) et miocène du Monte Capanne (Ile d'Elbe, Italie)*. Mémoires de Géologie de l'Université de Lausanne, **7**.
- BUSSY, F. & VON RAUMER, J. F. 1994. U–Pb geochronology of Palaeozoic magmatic events in the Mont Blanc crystalline massif, Western Alps. *Schweizerische Mineralogische und Petrographische Mitteilungs*, **74**, 514–515.
- BUSSY, F., SCHALTEGGER, U. & MARRO, C. 1989. The age of the Mont Blanc granite (Western Alps): a heterogeneous system dated by Rb–Sr whole-rock determinations on its microgranular enclaves. *Schweizerische Mineralogische und Petrographische Mitteilungs*, **69**, 3–13.
- BUTLER, R. W. H. 1985. The restoration of thrust systems and displacement continuity around the Mont Blanc massif, NW external Alpine thrust belt. *Journal of Structural Geology*, **7**, 569–582.
- CERIANI, S., FÜGENSCHUH, B. & SCHMID, S. M. 2001. Multi-stage thrusting at the 'Penninic Front' in the Western Alps between Mont Blanc and Pelvoux massifs. *International Journal of Earth Science*, **90**, 685–702.
- COX, S. F. 2005. Coupling between deformation, fluid pressures and fluid flow in ore-producing hydrothermal systems at depth in the Earth's crust. *Economic Geology 100th Anniversary Volume*, 39–75.
- COX, S. F., ETHERIDGE, M. A. & WALL, V. J. 1987. The role of fluids in syntectonic mass transport, and localization of metamorphic vein-type ore deposits. *Ore Geology Reviews*, **2**, 65–86.
- CRESPO-BLANC, A., MASSON, H., SHARP, Z., COSCA, M. & HUNZIKER, J. 1995. A stable and $^{40}\text{Ar}/^{39}\text{Ar}$ isotope study of a major thrust in the Helvetic nappes (Swiss Alps): evidence for fluid flow and constraints on the nappe kinematics. *Geological Society of America Bulletin*, **107**, 1129–1144.
- DEJONG, K. 2003. Very fast exhumation of high-pressure metamorphic rocks with excess ^{40}Ar and inherited ^{87}Sr , Betic Cordilleras, southern Spain. *Lithos*, **70**, 91–110.
- DEJONG, K., FÉRAUD, G., RUFFET, G., AMOURIC, M. & WIJBRANS, J. R. 2001. Excess argon incorporations in phengite of the Mulhacén complex: submicroscopic illitization and fluid ingress during late Miocene extension in the Betic zone, south-eastern Spain. *Chemical Geology*, **178**, 159–195.
- DODSON, M. H. 1973. Closure temperature in cooling geochronological and petrological systems. *Contributions to Mineralogy and Petrology*, **40**, 259–274.
- DUMONT, T., HEYMES, T., ROLLAND, Y. & AUTHEMAYOU, C. 2004. Early Oligocene N–NW thrusting in the External Alps before the onset of westward indentation. *2nd Swiss Geoscience Meeting*, Lausanne.
- DUNLAP, W. J. 1997. Neocrystallization or cooling? $^{40}\text{Ar}/^{39}\text{Ar}$ ages of white micas from low-grade mylonites. *Chemical Geology*, **143**, 181–203.
- DUNLAP, W. J. & KRONENBERG, A. K. 2001. Argon loss during deformation of micas: constraints from laboratory deformation experiments. *Contributions to Mineralogy and Petrology*, **141**, 174–185.
- FERRY, J. M. & GERDES, M. L. 1998. Chemically reactive fluid flow during metamorphism. *Annual Reviews in Earth and Planet. Science*, **26**, 255–287.
- FISCHER, H. & VILLA, I. M. 1990. Erste K/Ar- und $^{40}\text{Ar}/^{39}\text{Ar}$ -Hornblende-Mineralalter des Taveyannaz-Sandsteins. *Schweizerische Mineralogische und Petrographische Mitteilungs*, **70**, 73–75.
- FITZ GERALD, J. D. & STÜNITZ, H. 1993. Deformation of granitoids at low metamorphic grade. I: reactions and grain size reduction. *Tectonophysics*, **221**, 269–297.
- GIBSON, R. G. 1990. Nucleation and growth of retrograde shear zones: an example from the Needle mountains, Colorado, USA. *Journal of Structural Geology*, **12**, 339–350.
- GOODWIN, L. B. & RENNE, P. R. 1991. Effects of progressive mylonitization on Ar retention in biotites from the Santa Rosa mylonite zone (California), and thermochronologic implications. *Contributions to Mineralogy and Petrology*, **108**, 283–297.
- GOURLAY, P. 1986. La déformation du socle et des couvertures delphino-helvétiques dans la région du Mont Blanc (Alpes occidentales). *Bulletin de la Société Géologique de France*, **8**, 159–169.
- GOURLAY, P. & RICOU, L. E. 1983. Le jeu décrochant dextra Tardif de la suture de Chamonix (Alpes françaises et suisses). *Comptes Rendu de la Academie de Sciences Paris*, **296**, 927–932.
- GRASEMANN, B. & MANCKTELOW, N. S. 1993. Two-dimensional thermal modelling of normal faulting: the Simplon Fault Zone, Central Alps, Switzerland. *Tectonophysics*, **225**, 155–165.
- GUERMANI, A. & PENNACCHIONI, G. 1998. Brittle precursors of plastic deformation in a granite: an example from the Mont Blanc massif (Helvetic, western Alps). *Journal of Structural Geology*, **20**, 135–148.
- HAMES, W. E. & BOWRING, S. A. 1994. An empirical evaluation of the argon diffusion geometry in muscovite. *Earth and Planetary Science Letters*, **124**, 161–167.

- HAMES, W. E. & CHENEY, J. T. 1997. On the loss of $^{40}\text{Ar}^*$ from muscovite during polymetamorphism. *Geochimica Cosmochimica Acta*, **61**, 3863–3872.
- HAMES, W. E. & HODGES, K. V. 1993. Laser $^{40}\text{Ar}/^{39}\text{Ar}$ evaluation of slow cooling and episodic loss of ^{40}Ar from a sample of polymetamorphic muscovite. *Science*, **261**, 1721–1723.
- HUBBARD, M. & MANCKTELOW, N. S. 1992. Lateral displacement during Neogene convergence in the western and central Alps. *Geology*, **20**, 943–946.
- HUNZIKER, J. C., DESMONS, J. & HURFORD, A. J. 1992. *Thirty-two Years of Geochronological Work in the Central and Western Alps: a Review on Seven Maps*. Mémoires de Géologie de l'Université de Lausanne, **13**, 1–59.
- JOURDAN, F., FÉRAUD, G., BERTRAND, H., KAMPUNZU, A. B., TSHOSO, G., LE GALL, B., TIERCELIN, J. J. & CAPIEZ, P. 2004. The Karoo triple junction questioned: evidence for Jurassic and Proterozoic $^{40}\text{Ar}/^{39}\text{Ar}$ ages and geochemistry of the giant Okavango dyke swarn (Botswana). *Earth and Planetary Science Letters*, **222**, 989–1006.
- KELLEY, S. P. 1988. The relationship between K–Ar mineral ages, mica grain sizes and movement on the Moine Thrust Zone, NW Highlands, Scotland. *Journal of the Geological Society London*, **145**, 1–10.
- KELLEY, S. P. 2002. Excess argon in K–Ar and Ar–Ar geochronology. *Chemical Geology*, **188**, 1–22.
- KERRICH, R. 1986. Fluid infiltration into fault zones: chemical, isotopic, and mechanical effects. *Pure and Applied Geophysics*, **124**, 225–268.
- KIRSCHNER, D. L., COSCA, M., MASSON, H. & HUNZIKER, J. 1996. Staircase $^{40}\text{Ar}/^{39}\text{Ar}$ spectra of fine-grained white mica: timing and duration of deformation and empirical constraints on argon diffusion. *Geology*, **24**, 747–750.
- KIRSCHNER, D. L., MASSON, H. & COSCA, M. A. 2003. An $^{40}\text{Ar}/^{39}\text{Ar}$, Rb/Sr, and stable isotope study of micas in low-grade fold-and-thrust belt: an example from the Swiss Helvetic Alps. *Contributions to Mineralogy and Petrology*, **145**, 460–480.
- KLIGFIELD, R., HUNZIKER, J., DALLMEYER, R. D. & SCHAMEL, S. 1986. Dating deformation phases using K–Ar and $^{40}\text{Ar}/^{39}\text{Ar}$ techniques: results from the Northern Apennines. *Journal of Structural Geology*, **8**, 781–798.
- KRAMAR, N., COSCA, M. A. & HUNZIKER, J. C. 2001. Heterogeneous $^{40}\text{Ar}^*$ distributions in naturally deformed muscovite: *in-situ* UV–laser ablation evidence for micro-structurally controlled diffusion. *Earth and Planetary Science Letters*, **192**, 377–388.
- LELOUP, P. H., ARNAUD, N., SOBEL, E. R. & LACASSIN, R. 2005. Alpine thermal and structural evolution of the highest external crystalline massif: the Mont Blanc. *Tectonics*, **24**, TC4002, doi:10.1029/2004TC001676.
- LEUTWEIN, F., POTY, B., SONET, J. & ZIMMERMAN, J. L. 1970. Age des cavités à cristaux du granite du Mont Blanc. *Comptes Rendu de l'Académie de Sciences Paris*, **271**, 156–158.
- LO, C. H. & ONSTOTT, T. C. 1989. ^{39}Ar recoil artifacts in chloritized biotite. *Geochimica Cosmochimica Acta*, **53**, 2697–2711.
- MANCKTELOW, N. S. 1992. Neogene lateral extension during convergence in the Central Alps: evidence from interrelated faulting and backfolding around the Simplonpass (Switzerland). *Tectonophysics*, **215**, 295–317.
- MARÉCHAL, J. C. & PERROCHET, P. 2001. Theoretical relation between water flow rate in a vertical fracture and rock temperature in the surrounding massif. *Earth and Planetary Science Letters*, **194**, 213–219.
- MARKLEY, M. J., TEYSSIER, C., COSCA, M. A., CABY, R., HUNZIKER, J. C. & SARTORI, M. 1998. Alpine deformation and $^{40}\text{Ar}/^{39}\text{Ar}$ geochronology of synkinematic white micas in the Siviez–Mischabel Nappe, western Penninic Alps, Switzerland. *Tectonics*, **17**, 407–425.
- MARQUER, D. 1989. Transferts de matières et déformation des granitoïdes. Aspects méthodologiques. *Schweizerische Mineralogische und Petrographische Mitteilung*, **69**, 13–33.
- MARRO, C. 1988. Organisation géochimique et organisation du granite du Mont Blanc et de deux leucogranites. *Schweizerische Mineralogische und Petrographische Mitteilung*, **68**, 521–529.
- MARSHALL, D., PFEIFER, H. R., HUNZIKER, J. C. & KIRSCHNER, D. 1998. A pressure–temperature–time path for the NE Mont Blanc massif: fluid-inclusion, isotopic and thermobarometric evidence. *European Journal of Mineralogy*, **10**, 1227–1240.
- MCCAIG, A. M., WICKHAM, S. M. & TAYLOR, H. P. 1990. Deep fluid circulation in Alpine shear zones, Pyrenees, France: field and oxygen isotope studies. *Contributions to Mineralogy and Petrology*, **106**, 41–60.
- MCDUGALL, I. & HARRISON, M. T. 1999. *Geochronology and Thermochronology by the $^{40}\text{Ar}/^{39}\text{Ar}$ method*, 2nd edn. Oxford University Press, Oxford.
- MULCH, A., COSCA, M. A. & HANDY, M. R. 2002. *In-situ* UV–laser $^{40}\text{Ar}/^{39}\text{Ar}$ geochronology of a micaceous mylonite: an example of defect-enhanced argon loss. *Contributions to Mineralogy and Petrology*, **142**, 738–752.
- MÜLLER, W., MANCKTELOW, N. S. & MEIER, M. 2000. Rb–Sr microchrons of synkinematic mica in mylonites an example from the DAV fault of the Eastern Alps. *Earth and Planetary Science Letters*, **180**, 385–397.
- O'HARA, K. 1988. Fluid flow and volume loss during mylonitization: an origin for phyllonite in an overthrust setting, North Carolina, USA. *Tectonophysics*, **156**, 21–36.
- POTY, B. 1969. *La croissance des cristaux de quartz dans les filons sur l'exemple du filon de la Gardette (Bourg d'Oisans) et des filons du massif du Mont Blanc*. PhD thesis, Université de Nancy.
- POTY, B., STADLER, H. A. & WEISBROD, A. M. 1974. Fluid inclusion studies in quartz from fissures of the Western and Central Alps. *Schweizerische Mineralogische und Petrographische Mitteilung*, **54**, 717–752.
- RAMSAY, J. G. 1981. Tectonics of the Helvetic nappes. In: MCKLAY, K. R. & PROCE, N. J. (eds) *Thrust and Nappe Tectonics*. Geological Society of London Special Publications, **9**, 293–309.

- RAMSAY, J. G., CASEY, M. & KLIGFIELD, R. 1983. Role of shear in development of the Helvetic fold-thrust belt of Switzerland. *Geology*, **11**, 439–442.
- REDDY, S. M. & POTTS, G. J. 1999. Constraining absolute deformation ages: the relationship between deformation mechanisms and isotope systematics. *Journal of Structural Geology*, **21**, 1255–1265.
- REDDY, S. M., KELLEY, S. P. & WHEELER, J. 1996. A $^{40}\text{Ar}/^{39}\text{Ar}$ laser probe study of micas from the Sesia Zone, Italian Alps: implications for metamorphic and deformation histories. *Journal of Metamorphic Geology*, **14**, 493–508.
- ROLLAND, Y., CORSINI, M., ROSSI, M., COX, S. F., PENNACCHIONI, G., MANCKTELOW, N. & BOULLIER, A. M. 2007. Comment on the dating of Alpine deformation by Ar–Ar on syn-kinematic mica in mid-crustal shear zones of the Mont Blanc Massif (paper by Leloup *et al.*). *Tectonics*, **26**, TC2015, doi:10.1029/2006TC001956.
- ROLLAND, Y., COX, S. F., BOULLIER, A. M., PENNACCHIONI, G. & MANCKTELOW, N. 2003. Rare Earth and trace element mobility and fractionation in mid-crustal shear zones: insights from the Mont Blanc Massif (Western Alps). *Earth and Planetary Science Letters*, **214**, 203–219.
- ROSSI, M. 2005. *Déformation, transferts de matière et de fluide dans la croûte continentale: application aux massifs cristallins externes des Alpes*. PhD thesis, Université de Grenoble.
- ROSSI, M., ROLLAND, Y., VIDAL, O. & COX, S. F. 2005. Geochemical variations and element transfer during shear zone development and related epidyenites at middle crust depths: insights from the study of the Mont Blanc Granite (French-Italian Alps). In: BRUHN, D. & BURLINI, L. (eds) *High-strain Zones: Structure and Physical Properties*. Geological Society of London Special Publications, **245**, 373–396.
- SCAILLET, S. 1996. Excess ^{40}Ar transport scale and mechanism in high-pressure phengites; a case study from an eclogitized metabasite of the Dora–Maira nappe, Western Alps. *Geochimica Cosmochimica Acta*, **60**, 1075–1090.
- SEWARD, D. & MANCKTELOW, N. S. 1994. Neogene kinematics of the central and western Alps: evidence from fission-track data. *Geology*, **22**, 803–806.
- SHERLOCK, S., KELLEY, S. P., ZALASIEWICZ, J. A., SCHOFIELD, D. I., EVANS, J. A., MERRIMAN, R. J. & KEMP, S. J. 2003. Precise dating of low-temperature deformation: Strain-fringe analysis by ^{40}Ar – ^{39}Ar laser microprobe. *Geology*, **31**, 219–222.
- STECK, A. 1984. Structures de déformations tertiaires dans les Alpes centrales (transversale Aar–Simplon–Ossola). *Eclogae Geologicae Helveticae*, **77**, 55–100.
- STECK, A. & HUNZIKER, J. C. 1994. The tertiary structural and thermal evolution of the Central Alps – compressional and extensional structures in an Orogenic belt. *Tectonophysics*, **238**, 229–254.
- STEIGER, R. H. & JÄGER, E. 1977. Subcommittee on geochronology: convention of the use of decay constants in geo- and cosmochronology. *Earth and Planetary Science Letters*, **36**, 359–362.
- STREIT, J. E. & COX, S. F. 1998. Fluid infiltration and volume-change during mid-crustal mylonitization of Proterozoic granite, King Island, Tasmania. *Journal of Metamorphic Geology*, **16**, 197–212.
- TURNER, G., HUNEKE, J. C., PODOSE, F. A. & WASSERBURG, G. J. 1971. $^{40}\text{Ar}/^{39}\text{Ar}$ ages and cosmic ray exposure ages of Apollo 14 samples. *Earth and Planetary Science Letters*, **12**, 15–19.
- VILLA, I. M. 1998. Isotopic closure. *Terra Nova*, **10**, 42–47.
- VILLA, I. M., RUGGIERI, G. & PUXEDDU, M. 1997. Petrological and geochronological discrimination of two white-mica generations in a granite cored from the Larderello–Travale geothermal field (Italy). *European Journal of Mineralogy*, **9**, 563–568.
- VON RAUMER, J. F. 1974. Kristallization und Gefügebildung im Mont Blanc granit. *Schweizerische Mineralogische und Petrographische Mitteilung*, **47**, 499–579.
- WEST, D. P. & LUX, D. R. 1993. Dating mylonitic deformation by the ^{40}Ar – ^{39}Ar method: an example from the Norumbega Fault Zone, Maine. *Earth and Planetary Science Letters*, **120**, 221–237.
- WIBBERLEY, C. A. J. & MCCAIG, A. M. 2000. Quantifying orthoclase and albite muscovitisation sequences in fault zones. *Chemical Geology*, **165**, 181–196.
- WICKMAN, F. E., ABERG, G. & LEVI, B. 1983. Rb–Sr dating of alteration events in granitoids. *Contributions to Mineralogy and Petrology*, **83**, 358–362.
- WIJBRANS, J. R. & MCDUGALL, I. 1986. $^{40}\text{Ar}/^{39}\text{Ar}$ dating of white micas from an Alpine high-pressure metamorphic belt on Naxos (Greece) – the resetting of the argon isotopic system. *Contributions to Mineralogy and Petrology*, **93**, 187–194.